Biogeosciences Discuss., 10, 15951–16001, 2013
www.biogeosciences-discuss.net/10/15951/2013/
doi:10.5194/bgd-10-15951-2013

Biogeosciences Discussions
Open Access

Physical and remineralization processes govern the cobalt distribution in the deep western Atlantic ocean

G. Dulaquais[1], M. Boye[1], M. J. A. Rijkenberg[2,3], and X. Carton[4]

[1]Laboratoire des Sciences de l'Environnement Marin UMR6539, Institut Universitaire Européen de la Mer UMS3113, Technopôle Brest Iroise, Place Nicolas Copernic, 29280 Plouzané, France
[2]Department of Marine Biology, University of Groningen, P.O. Box 14, 9750 AA Haren, the Netherlands
[3]Department of Marine Chemistry and Geology, Royal Netherlands Institute for Sea Research, P.O. Box 59, 1790 AB Den Burg, the Netherlands
[4]Laboratoire de Physique des Océans, Université de Bretagne Occidentale – UFR Sciences, 6 avenue Le Gorgeu, C.S. 93837, 29238 Brest Cedex 3, France

Received: 6 September 2013 – Accepted: 11 September 2013 – Published: 16 October 2013

Correspondence to: G. Dulaquais (gabriel.dulaquais@univ-brest.fr)

Published by Copernicus Publications on behalf of the European Geosciences Union.

Abstract

The distributions of the bio-essential trace element dissolved Co (DCo) and the apparent particulate Co (PCo) are presented along the GEOTRACES-A02 deep section from 64° N to 50° S in the West Atlantic Ocean. PCo was determined as the difference between total cobalt (TCo, unfiltered samples) and DCo. DCo concentrations ranged from 14.7 pM to 94.3 pM, and PCo concentrations from undetectable values to 18.8 pM. The lowest DCo concentrations were observed in the subtropical domains, and the highest in the low-oxygenated Atlantic Central Waters (ACW) that appeared to be the major reservoir of DCo in the West Atlantic. In the Antarctic Bottom Waters, the enrichment in DCo with ageing of the water-mass can be related to suspension and redissolution of bottom sediments a well as diffusion of DCo from abyssal sediments. Mixing and dilution of deep water-masses, rather than scavenging of DCo onto settling particles, generated the meridional decrease of DCo along the southward large-scale circulation in the deep West Atlantic. Furthermore the apparent scavenged profile of DCo observed in the deep waters likely resulted from the persistence of relatively high concentrations in intermediate waters and low DCo concentrations in underlaying bottom waters. We suggested that the 2010 Icelandic volcanic eruption can be a source of DCo that could have been transported in the core of the North-East Atlantic Deep Waters. At intermediate depths, the high concentrations of DCo recorded in the ACW linearly correlated with the apparent utilization of oxygen (AOU), indicating that remineralization of DCo can be significant (representing up to 29 % of the DCo present). Furthermore the preferential remineralization of phosphate (P) compared to Co in these low-oxygenated waters suggested a decoupling between the deep cycles of P and Co. The vertical diffusion of DCo from the ACW appeared to be a significant source of DCo into the surface waters of the equatorial domain. Summarizing the dilution and mixing processes rather than scavenging of DCo, and the remineralization can be the two major pathways controlling the cycling of DCo in the intermediate and deep West Atlantic.

BGD
10, 15951–16001, 2013

1 Introduction

In the context of the international GEOTRACES program, unprecedent efforts are underway to map the distribution of trace elements and isotopes in the global oceans. Cobalt (Co) is among the important micro-nutrients highlighted in this program. Dissolved cobalt (DCo) typically occurs at concentrations lower than 150 pM in the open ocean (Knauer et al., 1982; Martin et al., 1990; Fitzwater et al., 2000; Saito and Moffett, 2001; Saito et al., 2004; Ellwood, 2008; Noble et al., 2008; Pohl et al., 2011; Bown et al., 2011), requiring sensitive analytical techniques for its detection (Vega and van den Berg, 1997; Cannizzaro et al., 2000; Saito and Moffett, 2001; Milne et al., 2010; Shelley et al., 2010). Previous studies suggest that DCo can be an hybrid-type metal (Bruland and Lohan, 2003; Noble et al., 2008), with a nutrient-like distribution in surface waters (Martin et al., 1993; Saito and Moffett, 2002; Saito et al., 2004; Jakuba et al., 2008; Noble et al., 2008; Saito and Goepfert, 2008; Bown et al. 2011) and a scavenged-type distribution in the deep ocean (Knauer et al., 1982; Wong et al., 1995; Noble et al., 2008; Boyd and Elwood, 2010). In surface waters, the organic complexation of cobalt can limit its scavenging onto settling particles and increase its bioavailability, notably to cyanobacteria (Saito and Moffett, 2001; Bown et al., 2012a). Cobalt and manganese (Mn) often cycle together through a removal pathway of co-oxidation with manganese driven by microbes, but the biological assimilation of DCo can uncouple the Mn-Co relationship in surface waters (Moffett and Ho, 1996). Furthermore, previous studies showed high DCo concentration in oxygen-depleted waters (Saito et al. 2004, 2005; Noble et al., 2012) that can be due to unfavorable microbial oxidation of DCo decreasing its scavenging rate (Noble et al., 2012). Moreover an experimental study on the oxidation processes of cobalt showed that the oxidation of Co is only occurring in the solid phase under anoxic and reductive conditions resulting in the desorption of Co from particles to solution (Behl and Toni, 1971). On the other hand the low solubility of inorganic Co in oxygenated waters and the affinity of DCo for particles have been invoked to explain DCo does not seem to accumulate in the deep-waters along

BGD
10, 15951–16001, 2013

the thermohaline circulation (Bruland and Lohan, 2003), and to interpret the apparent scavenged-type profile of DCo observed in the deep ocean (Aparicio-Gonzalez et al., 2012). In fact the scavenging of DCo onto settling particles and its stabilization in solution by the complexation with organic binding ligands could be the two major pathways controlling the internal cycling of Co in the deep ocean (Saito et Moffett, 2001, 2002). A residence time of 40–120 yr has been estimated for DCo in the deep ocean, that is more than two orders of magnitude longer than its residence time in surface waters (e.g. 0.32 yr; Saito and Moffett, 2002).

Despite these major findings our understanding of the biogeochemical cycle of cobalt in the ocean is still limited, notably in the West Atlantic Ocean where observations of the deep distribution of DCo are scarce. Biological uptake, recycling, scavenging and remineralization processes are suspected to strongly impact the distribution of DCo in the ocean (Saito and Moffett, 2002; Bown et al., 2011; Noble et al., 2008, 2012). Advection of water masses enriched in DCo following contact with continental margins can be a significant source of DCo to intermediate and deep waters (Wong et al., 1995; Saito et al., 2004; Noble et al., 2008; Bown et al., 2011). Others important sources of DCo to surface waters are river (Tovar-Sanchez et al., 2011) and atmospheric depositions (Shelley et al., 2012). Hydrothermal vents (Bruland and Lohan, 2003) and sediment resuspension can be important sources of DCo to the deep ocean (Bown et al., 2012a).

In this study the vertical and meridional distributions of DCo and apparent particulate cobalt (PCo), are presented along the GEOTRACES-A02 section in the West Atlantic Ocean from the East coast of the Greenland (64° N) to the Malvinas Plateau (50° S). The GEOTRACES-A02 transect is revisiting the Atlantic GEOSECS section of 1972, crossing distinct biogeochemical areas such as subtropical, equatorial or subpolar domains where different trophic chains are growing in each. Moreover this section also encounters several water masses involved in the thermohaline circulation and surface jets such as the north Atlantic drift known for its important role on climate regulation. This study focuses on processes that determine the intermediate and deep distribu-

BGD
10, 15951–16001, 2013

tions of DCo. In order to understand the vertical DCo distribution, its transportation across the entire West Atlantic Ocean is studied. Additionnaly, mechanisms governing the fractionation of Co between particulate and dissolved fractions are investigated. Finally, the impact of the meso-scale dynamics on the distribution of cobalt in surface waters is also discussed. The cycle and budget of DCo in the surface waters along the section are discussed elsewhere (Dulaquais et al., 2013). This large and deep section together with the relatively high spatial resolution gave us the opportunity to present, for the first time, the largest comprehensive dataset of cobalt in the West Atlantic ocean.

2 Methods

2.1 Cruise track and sampling

The samples were collected along the GEOTRACES-A02 section in the West Atlantic ocean, the longest section of the international GEOTRACES program. Four expeditions conducted between 2010 and 2012 were necessary to complete this section spreading from 64° N to 50° S along the West Atlantic Ocean (Fig. 1). Three cruises were operated aboard the Dutch R/V *Pelagia* (Legs 1-2-4) and one cruise aboard the British R.S.S. *James Cook* (Leg 3). The first cruise started in May 2010 from 64° N to Bermuda in the Sargasso Sea (St. 1–19), followed by the second leg from the station BATS to the Equator (St. 21–41). The section in the South West Atlantic (Leg 3) from 50° S to the Equator was achieved in 2011 (St. 1b–18b). An additional cruise (Leg 4) was operated in 2012 to complete the first leg fragmented due to bad weather (St. 3c–7c).

A total of 47 stations with a vertical resolution of 12–16 depths between 9 m and 5930 m were sampled for dissolved cobalt analyses (DCo), and 15 stations for total (unfiltered) cobalt determinations (TCo). The apparent particulate cobalt concentrations (PCo) were calculated by substraction of DCo from TCo. The complete dataset of cobalt (dissolved, total, and apparent particulate) at all stations will be available at the international GEOTRACES datacenter (http://www.bodc.ac.uk/geotraces/).

BGD
10, 15951–16001, 2013

Samples were taken using the TITAN-CTD frame of NIOZ (Netherlands), with 24 ultra-clean sampling bottles of 24.4 L each made of PVDF plastic (de Baar et al., 2008). The frame was placed in a Class-100 container for sub-sampling (de Baar et al., 2008). Unfiltered samples were transfered into acid cleaned 250 mL Nalgene® LDPE bottles for TCo analyses. The samples for DCo analyses were collected after filtration using 0.2 µm Sartobran® 300 (Sartorius) cartridges under pure N_2 pressure (filtered 99.99 % N_2, 0.7 atm) in acid cleaned 250 mL or 500 mL Nalgene® LDPE bottles. All samples were acidified at pH ∼ 2 using ultrapure HCl® (Merck) immediately after their collection. Then the acidified samples were stored in double bags at dark and ambient temperature, before their analyses in the shore-based laboratory.

2.2 Analytical method for cobalt analyses

2.2.1 Method

Prior to the analyses, the samples were UV-digested (Saito and Moffet, 2002; Shelley et al., 2010) for 3 h in acid clean silica tubes using a 600 W high-pressure mercury vapor lamp (Bown et al., 2011), and left for an equilibration time of 48 h. Preliminary tests indicated that 3 h of UV-digestion were required to fully recover Co in surface and deep samples (data not shown).

Dissolved and total cobalt concentrations were determined by Flow-Injection Analysis (FIA) and chemiluminescence detection following the method adapted from Shelley et al. (2010), as described in Bown et al. (2011). In this method, cobalt catalyzes the oxidation reaction of pyrogallol with hydrogen peroxide in an alkaline solution in the presence of cetylmethylammoniumbromide (CTAB) and methanol. A chemiluminescent emission in the visible wavelengths proportional to the cobalt concentration is produced during this reaction. The system consists of one 10-ports injection valve (VICI valves from VALCO instruments) which operates as an autosampler, and of two micro-electronically actuated injection valves (VICI valves from VALCO instruments) to

BGD
10, 15951–16001, 2013

inject the sample and the reagents using Tygon® tubes. The flow injection is provided by a peristaltic pump (205 CA, Watson Marlow).

The reagents are prepared with trace metals quality reagents, as described in Bown et al. (2011). All reagents are prepared under a laminar flow hood (ADS Laminaire, ISO 5 class) in 1 L LDPE Nalgene® bottles with ultrapure water (MiliQ, 18.2 mΩ) the day before the analysis and kept at room temperature for an overnight equilibration.

The sample is buffered online with ammonium acetate (0.3 M, ACS Reagents), and load on an IDA-Toyopearl chelating resin to preconcentrate the cobalt contained in the sample. Then a HCl solution (0.1 M, Suprapur® Merck) is injected through the column to elute Co. The elutant is warmed in a 60 °C thermostatic bath to limit the interferences in the detection system due to bubbles (Shelley et al., 2010). The detection system consists of a photomultiplier detector (Hamamatsu, H9319 Series). The injection valves and the photomultiplier detector are operated on a laptop by a modified Labview® 8.4 interface (E. Duvieilbourg and M. Boye, LEMAR). The electrical devices are connected to a modulator of current (ELLIPSEMAX 600, MGE/UPS Systems).

The Co concentrations were calibrated against two calibration curves made with standard additions of cobalt of 0, 12.5, 25, 50 and 75 pM to seawater, and performed before and after each series of 8 or 12 samples. TCo and DCo concentrations are based on triplicate analyses of each sample using the mean peak height of the chemiluminescent signal, and they are corrected with respect to blank analyses. Two to four reagent blanks including the buffer blank were analyzed per series of 8–12 samples at the beginning and at the end of the series, in acidified MilliQ water instead of the sample (Bowie and Lohan, 2009; Bown et al., 2010). DCo and PCo concentrations shown in this study are corrected with their respective reagent blanks.

The final standard deviation of the measurement is calculated by an error propagation using the error on blanks, the calibration curves and the deviation of the triplicate analyses. A *t* test was applied to verify that the difference between TCo and DCo is significant to allow reliable estimation of PCo concentration. The standard er-

BGD
10, 15951–16001, 2013

ror on PCo is calculated by combining uncertainties of DCo and TCo measurements ($SD_{PCo} = (SD^2_{DCo} + SD^2_{TCo})^{0.5}$).

2.2.2 Analytical performance

The mean reagent blank (based on all blank determinations) was 4.2 ± 2.1 pM of Co in MilliQ ($n = 180$). The limit of detection of the method estimated as the mean reagent blank added to three times the standard deviation (e.g. 6.3 pM) is thus on average 10.5 pM of Co ($n = 180$). Each series of samples was calibrated by running one or two samples collected during the Sampling and Analysis of iron (SAFe) program or GEOTRACES program. SAFe and GEOTRACES samples were UV-digested for 3 h prior to analysis and the results of DCo concentrations are reported in Table 1. The DCo concentrations we measured in the SAFe and GEOTRACES reference-samples are in excellent agreement with the consensus values http://www.geotraces.org/science/intercalibration/322-standards-and-reference-materials. The DCo value obtained in the S-SAFe sample also falls in the consensus value despite the concentration being lower than the detection limit. The analytical precision of the method was determined from repeated analyses of the surface S-GEOTRACES reference-sample, yielding an uncertainty of ±3.8 % expressed as relative standard deviation on the mean ($n = 15$).

2.3 Hydrography

Hydrological parameters (S, T °, O_2, conductivity, fluorescence and turbidity) were measured using a SBE9+ underwater sensor, a SBE3+ thermometer (±0.001 °C), a SBE4 conductivity sensor (±0.3 mS s^{-1}), a SBE43 dissolved oxygen sensor ±2 %), a Chelsea Aquatracka MKIII fluorometer ±0.2 µg L^{-1}), and a Wetlabs C-Star transmissiometer ±0.02 % °C^{-1}; 25 cm, deep, red).

BGD
10, 15951–16001, 2013

2.4 Macronutrients analysis

Nutrient samples were collected in 125 mL polypropylene bottles using a CTD-rosette (Seabird® equipped with Niskin bottles. The analyses were performed onboard from surface to deep waters samples. All the nutrients were analyzed by colorimetric methods following the methods of Riley and Murphy (1962) for phosphate (HPO_4^{2-}), of Strickland and Parsons (1968) for silicate ($Si(OH)_4^-$), and of Grasshoff et al. (1983) for nitrate (NO_3^-) and nitrite (NO_2).

3 Results

3.1 Circulation and dynamic structures

In the North, the section crossed the Sub-Arctic Gyre (SAG) between 64° N and 50° N, where the Labrabor Sea Water (LSW) dives to form, with the Arctic Bottom Water, the Western North Atlantic Deep Water (WNADW). Deeper, the Eastern North Atlantic Deep Water (ENADW) is also isolated in the SAG and forms, further south, with the WNADW the North Atlantic Deep water (NADW) (Fig. 2). The well oxygenated and dense waters of the subarctic gyre are separated, in the south, from to relatively low-oxygenated, saline and warm waters of the North Atlantic Subtropical Gyre (NASG) by the North Subtropical Front (NSTF) at ~45° N. The NSTF is characterized by a high anomaly of temperature (+5 °C) and by a strong eastward geostrophic current in surface waters (data not shown) which is likely to be the North Atlantic Drift (Reid, 1994).

In the NASG, low-density waters occur in the top 600 m due to relatively high salinity and temperature (T ° > 10 °C; S > 35) (Fig. 2). However at 15° N and in a lesser extend at 4° N these saline waters were covered by relativey fresh waters (Fig. 2), originating from the Amazon plume. The waters influenced by the Amazon plume were characterized by relatively high Si : N ratio and turbidity (data not shown).

BGD
10, 15951–16001, 2013

Leaving the NASG southwards, the section enters in the equatorial area. Here the zonal geostrophic velocities indicate the presence of several jets at near of the surface, such as the North Equatorial Current (NEC, at 5–10° N), the North Equatorial Counter-Current (NECC, at ∼3° N), the South Equatorial Current (SEC, at 5–10° S) and the South Equatorial Under-Current (SEUC, at ∼5° S, 200 m depth) as described by Peterson and Stramma (1991). The equatorial domain is bordered by the NEC in the North and by the SEC in the South, both of which were characterized by westward surface geostrophic propagating vectors and similar speed (respectively 0.2 and 0.15 m s^{-1}). Below 100 m, the salinities and temperatures were lower than in the NASG revealing denser waters. An oxygen minimum zone (OMZ; $O_2 < 150$ µM) was also observed under these surface currents, between 150 and 600 m (Fig. 2c). Part of this low O_2-signature was due to the advection of the poorly oxygenated Atlantic Central Waters ($O_2 < 50$ µM; Noble et al., 2012), flowing westward from the African border across the Atlantic basin.

Southward the section enters into the South Atlantic Subtropical Gyre (SASG) characterized, like in the North, by low-density waters associated with relatively high salinities and temperatures (Fig. 2a–b). Despite strong eddy activity in this area, clearly observed in the geostrophic current field, the Malvinas-Brazil confluence (MBC), an eastward jet resulting from the Brazil current flowing southward and the Malvinas current flowing northward, can be located in the Argentine basin around 40° S (e.g. at station 6b; data not shown). The MBC separates the SASG with saline and relative oxygen-poor waters from the Subantarctic Waters (SAW).

Several water-masses involved in the large-scale ocean circulation were characterized at depth (Fig. 2). For instance the LSW was characterized by $34.9 < S > 34.8$ and $O_2 > 275$ µmol kg^{-1} in the Subarctic Gyre at 60° N (Fig. 2). The ENADW ($S > 34.925$) circulates underneath the LSW, following the topography below 2500 m in the northern side of the section. The core of the ENADW is situated between 62° N and 45° N. The WNADW and the ENADW both form the NADW spreading southward in the deep ocean from 60° N to 37° S (Tomczak and Godfrey, 2003). The Antarctic Bottom Water

BGD
10, 15951–16001, 2013

(AABW) characterized by $S < 34.8$ and $T^\circ < 1\,^\circ$C is formed in the Weddell Sea (Reid, 1989; Gladyshev et al., 2008) and spreads at the bottom of the ocean below 4000 m. The AABW enters the Atlantic Ocean by the south and follows the topography until 3° N. To the north the bottom waters are a mix between AABW, Arctic Bottom Waters (ABW) and NADW (Tomczak and Godfrey, 2003). In the southern hemisphere, the relative fresh Antarctic Intermediate Waters entering from the Drake Passage (D-AAIW; $S > 34.2$) are identified at intermediate depths between 500 and 1000 m. Finally, the oxygen distribution enables to distinguish the different components of the Circumpolar Deep Waters (CDW; Whitworth and Nowlin, 1987), with its upper component (UCDW) at about 1500 m marked by $O_2 < 190\,\mu mol\,kg^{-1}$, and its intermediate component (ICDW) at about 2500 m with $O_2 > 210\,\mu mol\,kg^{-1}$ (Fig. 2c). The intermediate waters in the equatorial domain are formed by a mix of AAIW and UCDW that both flow northward and of the Atlantic Central Waters (ACW) originated from the East Atlantic basin (Poole and Tomczak, 1999). However it has to be noted that the transitions between the different water masses vary with the latitude (Fig. 2).

3.2 The nutrients distribution along the section

Different biogeochemical domains were characterized in surface waters along the section (Fig. 3). The surface waters of the SAG were marked by relatively high phosphate and nitrate concentrations ($NO_3 > 10\,\mu M$; $PO_4 > 0.8\,\mu M$). In the two subtropical domains the extremely low nutrients concentrations (such as observed in the NASG where $PO_4 < 0.5\,\mu M$, $NO_3 < 5\,\mu M$, $Si < 5\,\mu M$) were characteristic of oligotrophic conditions. However a greater depletion of nitrogen relative to phosphate was observed in the upper 300 m of the SASG ($N:P < 10$) compared to the NASG ($N:P > 25$) probably due to a greater proportion of N_2 fixers, such as diazothrophic cyanobacteria, in the NASG than in the SASG (Mather et al., 2008). In the equatorial area, the intermediate waters are characterized by relatively high concentrations of nitrate and phosphate ($NO_3 > 34\,\mu M$, $PO_4 > 2.3\,\mu M$), whereas silicate concentrations were low ($5\mu M < Si < 15\,\mu M$), suggesting the incursion of D-AAIW formed in the south-western

BGD
10, 15951–16001, 2013

Atlantic. South of the South Subtropical Front, the nutrients distribution showed, as for oxygen, the influence of the AAIW and UCDW with relative high nutrient concentrations in the top 200 m depths ($NO_3 > 20\,\mu M$, $PO_4 > 1.2\,\mu M$). In the deep ocean the nutrients distribution reflected a combination of ageing and advection of water-masses (Fig. 3). The spreading of young NADW can be followed with the low-nutrients signature ($Si < 35\,\mu M$; $NO_3 < 20\,\mu M$; $PO_4 < 1.5\,\mu M$). Phosphate and nitrate concentrations increase southward in the deep ocean (Fig. 7), due to mixing of Arctic waters (poor in nutrients) with nutrients-enriched Antarctic waters. The AABW is characterized by relatively high nutrients concentrations ($Si > 130\,\mu M$; $NO_3 > 30\,\mu M$; $PO_4 > 2\,\mu M$) that decrease northward. The nutrient concentrations in the Circumpolar Deep Waters are similar to those of AABW, but the concentrations in the ICDW were a little bit lower than those in the UCDW. The silicate levels are depleted in the AAIW compared to others Antarctic waters.

3.3 The comprehensive distribution of cobalt in the West Atlantic

The meridional and vertical distributions of DCo along the section are presented in Fig. 4a. Dissolved cobalt concentrations range from 14.72 ± 1.43 to 93.27 ± 3.31 pM along the section. The lowest concentration was observed in surface waters of the SASG (e.g. at 9 m depth at St.#11b–26° S) whereas the highest were recorded in the OMZ of the equatorial area (e.g. at St.#15b–9° S at 290 m depth). The vertical distributions of the apparent particulate cobalt concentrations (PCo) calculated as the difference between the unfiltered and the filtered (< 0.2 µm) analyzed fractions, are presented in Fig. 4b. The apparent particulate cobalt concentrations ranged from near undetectable values (e.g. the difference between unfiltered and filtered samples analyses is not significant) to 18.85 ± 3.97 pM (e.g. at St.#17–34.3° N at 5510 m depth). PCo / DCo ratio range from 0.06 % (St. 17; 2500 m) to 44 % (St. 26, 25 m),with a mean of 7 % ($n = 192$).

Different vertical distributions of DCo were observed in each biogeochemical domain (Figs. 4–5). The distribution of DCo showed an apparent scavenged-like profile in the

BGD
10, 15951–16001, 2013

northern subarctic gyre (Figs. 4a–5a), with relatively higher concentrations in surface waters ($DCo_{upper\ 200\ m} > 70$ pM) compared to deeper waters ($DCo_{below\ 2000\ m} < 60$ pM). In this domain, lower surface DCo concentrations were recorded in 2012 during leg-4 (e.g. 42.1 ± 2.15 pM at St.#3c, and 44.23 ± 1.26 pM at St.#4c, at 25 m depth) compared to those observed in 2010 during leg-1 (e.g. mean DCo = 64.56 ± 5.25 pM at 25 m ($n = 4$), with a DCo maximum of 68.2 ± 1.08 pM at St.#5). At intermediate depths (500–1000 m) the LSW was characterized by relatively high DCo concentrations (DCo ~ 70 pM) compared to those found in the ENADW (DCo ~ 55 pM below 2000 m). In this domain, the apparent particulate cobalt distribution showed relative PCo maxima in the subsurface (ranging from 5.9 ± 1 to 10.4 ± 1.96 pM), and decreasing concentrations with depth (until undetectable levels around 1500 m depth). Maxima of PCo (> 10 pM) were then observed near the bottom (at St.#2&11).

In contrast, DCo was depleted in the surface waters of the two subtropical domains and increased with depth below the nutricline, featuring a nutrient-like distribution (Figs. 4a–5b). However, DCo are slightly lower and shallower in the SASG (mean DCo value of 23.01 ± 4.17 pM, $n = 9$) compared to those found in the NASG (mean DCo value of 28.8 ± 4.8 pM, $n = 15$). Subsurface relative maxima of DCo were observed at about 10 m depth at a few stations in the NASG. Deep relative DCo maxima were also observed at around 1250–1750 m depth in the NASG, that are in the core of NADW and below the oxygen minima. On the contrary relative DCo maxima and oxygen minima were often locate at the same depth in the SASG, within the core of the mixed NADW. In the AABW of the SASG, DCo was on average equal to 42.8 ± 2.23 pM ($n = 15$). In the two subtropical gyres, the PCo concentrations ranged from undetectable value (e.g. at 2500 m of St.#17) to 18.85 ± 3.97 pM (at 5510 m – 34.3° N). Like in the northern latitudes, relatively high PCo concentrations were observed in the surface waters, decreasing with depth, and increasing again near the seafloor (Fig. 5e). The PCo distribution also showed, like DCo, relatively lower PCo concentrations in the subsurface waters of the SASG (< 5 pM) compared to the NASG (> 5 pM).

BGD
10, 15951–16001, 2013

In the equatorial area, the DCo distribution was characterized by low concentrations in the top 100 m (mean $DCo_{\int 100\,m} = 29.6 \pm 9$ pM, $n = 44$), a sharp increase between 100 and 250 m (mean $DCo_{\int 100-250\,m} = 61.7 \pm 13$ pM, $n = 10$), that continued to increase to reach maximum values at about 400 m depth (mean $DCo_{\int 250-400\,m} = 73.2 \pm 10$ pM, $n = 19$) (Figs. 4–5c). These maximum concentrations were the highest values recorded along the section and reached values up to 93.27 ± 3.31 pM (at 9° S). Furthermore these DCo maxima strongly correlated with the oxygen depletion ($\Delta DCo/\Delta O_2 = -0.28\,\mu M\,M^{-1}$, $R^2 > 0.66$). Between 1000 and 2500 m depth, the DCo concentrations were in the same range as those observed at 100–250 m depths (mean $DCo_{\int 1000-2500\,m} = 67.6 \pm 5.8$ pM, $n = 33$). Deeper DCo concentrations decrease to a mean value of 41 ± 4 pM ($n = 15$) below 4000 m. The distribution of PCo in the equatorial domain was similar to that observed in the other domains, with several extremely low (undetectable) values in deep waters and relatively higher concentrations (PCo < 5 pM) in surface waters, up to a maximum value of 10.24 ± 2.1 pM observed at 10 m at St.#40 (1.15° N). A different pattern was however observed in the deep waters at 8° N (St. 36), where significant and increasing PCo concentrations were detected between 3500 m (1.52 ± 0.7 pM) and 4315 m (11.73 ± 1.9 pM), as well as at 3° S (St.#17b) where extremely high PCo concentrations were measured at 3500 m depth (12.53 ± 2.4 pM). In the surface waters, high PCo concentration (~ 10 pM) is measured at 1° N (St.#40) in the Amazon plume.

In the area of the Brazil-Malvinas confluence, DCo increased southward in the surface waters. The vertical distribution showed the highest DCo concentrations in the core of D-AAIW (100–600 m; Fig. 4a), whereas DCo levels decrease in deeper waters, generating an apparent scavenged-type distribution at latitudes of 49–49.5° S (St.#1b–2b). The DCo concentrations observed in the youngest-AABW flowing in this area were the lowest values recorded in the core of the AABW along the section ($DCo_{\int 4000-6000\,m} = 34.9 \pm 3$ pM). Only one profile of PCo has been analyzed in this area at 49° S (St.#2b). It showed relatively high PCo concentrations in the upper 300 m

BGD
10, 15951–16001, 2013

(PCo > 6 pM), and, as for the other domains, undetectable PCo concentrations in deep-waters, except at 5000 m where PCo reached a maximum (11.8 ± 3.4 pM).

4 Discussion

The scientific objective of this paper is to examine the spatial distributions of cobalt and its transportation along the entire West Atlantic Ocean. Firstly intercomparison between this dataset and others at three stations located in different biogeochemical domains will be presented. Then the cobalt distributions within the different water masses, in distinct geographic areas, will be discussed. In addition, the potential effect of 2010 Icelandic volcano Eyjafjallajökull eruption on the distribution of DCo will be discussed. The previous observation of cobalt transportation in the central-eastern Atlantic OMZ that suggests no scavenging process (Noble et al., 2012) motivated us to investigate the relationship between remineralization, scavenging and the decoupling of cobalt and phosphate in the O_2 depleted waters of the western central Atlantic. Finally in a meso-scale approach, the effect of dynamic structures on the surface DCo transportation and their impact on diffusion process will be considered.

4.1 Comparison of datasets of dissolved cobalt concentrations obtained at three crossover stations

Three crossover stations were occupied along the GEOTRACES-A02 section, at the Bermuda Atlantic Time Series BATS station (64.17° W–31.7° N), at 9° S during the US CoFeMUG cruise in 2007, and at 40° S during the English GEOTRACES-A10 section in 2012 (Fig. 6).

Station BATS in the Sargasso Sea was occupied on 13 June 2010 during our GA02-section (St.#21). The DCo concentrations analyzed by FIA-chemiluminescence method (this study, Figs. 6a and d: blue diamonds), are compared to those obtained by ICP-MS methods either in the same samples (Middag et al., 2013; Fig. 6a and d: yellow dots), or

BGD
10, 15951–16001, 2013

during other sampling cruises (Biller and Bruland, 2012: green triangles in Fig. 6a and d; Middag et al., 2013: red squares in Fig. 6a and d). All samples were analyzed after UV treatment. In the deep waters, no significant differences were observed between the different datasets, even when samples were taken in different years. On the contrary, differences were observed in surface waters (25–200 m), with systematic higher DCo values using the ICP-MS compared to the FIA-Chem. method. It is possible that seasonal variability, especially of atmospheric inputs to surface waters, would cause those variations of DCo levels recorded in surface waters (Biller and Bruland, 2012; Middag et al., 2013; Fig. 6a and d: green triangles and red squares, respectively). However further investigations are needed, because differences are also observed in the same set of samples (this study; Middag et al., 2013: yellow dots in Fig. 6a and d), yielding an offset of 6–20 pM DCo in the top-100 m between the ICP-MS method and FIA-Chem. analyses.

At 9° S, the DCo concentrations analyzed by FIA-chemiluminescence in the samples collected during the GA02-section (23 March 2011, St.#15b, this study) were compared with data analyzed by Cathodic Stripping Voltametry after UV-treatment, but in non-acidified samples (Noble et al., 2012). Despite the fact that the two stations are not exactly at the same location and that they were sampled in different years, the hydrography and the nutrient distributions were similar (data not shown) allowing for the comparison of the DCo datasets. The comparison showed an excellent correlation ($R^2 > 0.98$; Fig. 10e), suggesting that both analytical methods were in good agreement.

At 40° S, the two DCo datasets sampled during the GA02-section (10 March 2011, St.#6b, this study) and the GA10-section (January 2012; Lohan et al., 2013) were obtained using similar FIA-chemiluminescence methods after UV-digestion of the acidified sample. It showed an excellent agreement between the two datasets in the upper 3000 m (Fig. 6c and f), and an offset of 8–15 pM in the deepest waters below 3000 m (Fig. 6c). Because the analytical methods and sample treatments were similar, variability of the DCo concentrations in the relatively young AABW can be invoked to explain

BGD
10, 15951–16001, 2013

this difference. Further investigation is needed to determine the sources of this difference.

4.2 Large-scale transportation of dissolved cobalt in the West Atlantic

The behavior of DCo in the deep ocean is still poorly understood due to the lack of observations in the full water-column, notably in the West Atlantic Ocean, as well as in the Indian and the central Pacific oceans. The few studies that report DCo concentrations in the deep ocean suggest a decrease of DCo levels in the deep waters from the Atlantic Ocean (80.8 pM), to the Southern Ocean (39.7 pM), and to the Pacific (28.8 pM) (Bown et al., 2011; Aparicio-Gonzalez et al., 2012). This leads to the hypothesis there is no accumulation of DCo along the thermohaline circulation, and to classify DCo amongs either the scavenged-type element like aluminium (Aparicio-Gonzalez et al., 2012) or the hybrid-type metals, those elements strongly influenced by scavenging processes in deep waters (Noble et al., 2008). However the scavenging of DCo invoked to interpret the deep inter-basins fractionation is paradoxical with DCo known to be stabilized in solution by strong complexation with organic ligands (conditional stability constant, K_{CoL}, $> 10^{13}$) (Saito and Moffett, 2001; Saito et al., 2004, 2005, 2010; Bown et al., 2012a). On the other hand other processes, such as mixing of water-masses, have also been suggested to account for the decrease of DCo along water-masses circulation in the deep ocean (Noble et al., 2012). In this paragraph we investigate the behavior of DCo along the water-masses transportation in the deep and intermediate West Atlantic.

4.2.1 Transportation in bottom waters within the core of AABW

The Antarctic Bottom Waters spread northward with transport 2.5 and 5 Sv (where 1 Sv is equal to 10^6 m^3 s^{-1}) following the topography, in an opposite direction to the overlaying NADW (Tomczak and Godfrey, 2003). The mean DCo concentration in the AABW below 4000 m is 41.75 ± 5.3 pM along the whole transect ($n = 87$), but higher DCo levels are found in the older-AABW flowing in the Northern Hemisphere than in the more

BGD
10, 15951–16001, 2013

recently formed-AABW flowing in the South (mean values of 44.52 ± 4.8 pM, $n = 42$; and 39.29 ± 4.4 pM, $n = 45$, respectively). At the same southern latitudes, DCo concentrations were similar to those reported in the core of the recently formed AABW, but in the Eastern Atlantic Ocean (Bown et al., 2011; Table 2). Similar northward bottom enrichment of DCo in the core of AABW (Fig. 7a), together with water-mass pathway and ageing, has also been observed in the Eastern Atlantic sector (Bown et al., 2011). Enrichment due to mixing of the AABW with the NADW in the Subarctic basin is unlikely since DCo display similar concentrations in the cores of these two water-masses (Table 2). Bottom enrichment due to resuspension of abyssal sediments and their dissolution during AABW transportation is more likely to account for the northward increase of DCo. Such enrichment of DCo in waters following contact with basaltic sediments has recently been highlighted on the Kerguelen Plateau (Bown et al., 2012b). The significant increase of PCo observed close to the seafloor in the northern hemisphere (Fig. 5), rising up to 30 % of the total cobalt concentration at 34° N, also suggests that sediment resuspension could be significant. This is further supported by the strong signal of high dissolved aluminium concentrations observed in the bottom waters of the northern section (40–50° N) (R. Midagg, NIOZ, personal communication, 2013). Additionaly there was no record of high DCo at the bottom of the Mid Atlantic Ridge (Fig. 4a), suggesting that hydrothermal activity may not be acting as a significant source of DCo, as previously shown (Bown et al., 2011).

4.2.2 Transportation in the core of the NADW

Comparison of the DCo concentrations recorded in this study in the cores of the NEADW, NADW and D-AAIW with those reported in the south-eastern Atlantic (Bown et al., 2011) shows an excellent agreement (Table 2). This comparison suggests that DCo may not be scavenged during zonal (eastward) transportation across the South Atlantic at intermediate and deep depths.

To investigate the meridional (southward) transportation of DCo across the deep West Atlantic Ocean in the core of the NADW, this water-mass was characterized

BGD
10, 15951–16001, 2013

along its route southward, with respect to its mean DCo concentrations at three different potential density anomaly, corresponding to its center ($\sigma 0 = 27.85 \pm 0.02$), its upper-limit where the NADW interacts with intermediate waters (e.g. $\sigma 0 = 27.65 \pm 0.1$), and its lower-limit in contact with bottom waters (e.g. $\sigma 0 = 27.89 \pm 0.015$) (Fig. 7b). No significant variations are observed along these isopycnes from the Subarctic Gyre to the Equatorial area (e.g. DCo = 68.7 ± 6 pM, $n = 62$ at $\sigma 0 = 27.65$; 58.8 ± 3 pM, $n = 19$ at $\sigma 0 = 27.85$; 56.9 ± 7 pM, $n = 21$ at $\sigma 0 = 27.89$), suggesting conservative behavior of DCo in the NADW. Around the equator DCo concentration increased at two potential density (71.4 ± 4.4 pM $n = 10$ at $\sigma 0 = 27.65$; 62.6 ± 5 pM, $n = 14$ at $\sigma 0 = 27.85$) and decrease in the denser waters (DCo = 51.9 ± 8 pM, $n = 20$ at $\sigma 0 = 27.89$). There was no variation of PCo in this area at $\sigma 0 = 27.65$ and $\sigma 0 = 27.85$, and an increase of PCo at $\sigma 0 = 27.89$ (by 4.6 pM), all suggesting that remineralization of PCo could not be directly related to the increases in DCo at those depths. Hence the enrichment of DCo in the upper NADW may be more likely due to mixing with the overlaying Western Atlantic Central Water (W-ACW), containing relatively high DCo concentrations (> 85 pM).

Southward, the concentrations of DCo and PCo in the three layers were similar to those observed in the Equatorial area until 20° S ($\sigma 0 = 27.88$) or 30° S (along $\sigma 0 = 27.65$ and $\sigma 0 = 27.85$) (Fig. 7), again suggesting that DCo behaves conservatively at those southward latitudes. However, south of 20° S, a decrease of DCo concentrations was observed along the three isopycnes (Fig. 7). This decrease was more pronounced at the upper- and lower-limits than in the center of the NADW (e.g. the difference of concentrations between the North and the South Atlantic are: $\Delta DCo_{\sigma 0 = 27.65} = -11.5$ pM; $\Delta DCo_{\sigma 0 = 27.85} = +1.5$ pM; $\Delta DCo_{\sigma 0 = 27.89} = -10.3$ pM). There was no variation in the PCo concentrations associated with the decreases in DCo at the three depths (Fig. 4b), again suggesting that scavenging of DCo onto particles is not likely. Mixing and dilution of the NADW with the overlaying waters (D-AAIW in the upper-limit, and AABW in the lower layer) containing lower concentrations of DCo (Table 2) are thus more likely to explain the DCo decrease. Since mixing is stronger at the edges

BGD
10, 15951–16001, 2013

of the water-masses, the center of the NADW would be less impacted by such mixing effect.

We further investigate the effect of water-masses mixing on the southward DCo gradients along the NADW by calculating the DCo concentrations resulting from the dilution of intermediate and deep water-masses. In the northern section, the NADW is formed by mixing 5 Sv of LSW with a mean DCo concentration of 68.8 ± 3.17 pM ($n = 38$; Table 2), with 10 Sv of NEADW with a mean DCo concentration of 54.3 ± 2.69 pM ($n = 24$; Table 2) (Tomczak and Godfrey, 2003). The resulting theoretical concentration of DCo of 59.13 pM compared perfectly with the mean DCo concentration as observed in the NADW (61.4 ± 7.8, $n = 204$; Table 2). In the equatorial area, the mixing of 15 Sv of the NADW with the 4 Sv of the W-ACW (Schmitz, 1995) leads to a theoretical DCo concentration of 66.1 pM, which is in excellent agreement with our measurements in this area (DCo = 65.3 ± 7, $n = 43$). The slight increase observed in the DCo concentration of the NADW in this area can thus be due to mixing between the high DCo concentrations of the Western-ACW and the NADW, and to vertical diffusion. The vertical mixing occurs through internal waves that can provide a mix of more than half of the NADW (up to 8 Sv) (Webb and Suginohara, 2001). Along the southward flow of the NADW in the Southern Hemisphere, the DCo concentrations are higher than in the north (DCo = 63.7 ± 7 pM, $n = 23$) until 30° S, beyond which a strong decrease is observed (DCo = 54.6 ± 7 pM, $n = 45$). Here, the penetration of the 2.7 Sv of D-AAIW (You, 2002) in the intermediate ocean, and the 5 Sv of AABW in the deep sea (Tomczak and Godfrey, 2003) leads to a theoretical DCo concentration of 54 pM in the NADW, which is in excellent agreement with the concentration we measured in the NADW for this area (54.3 ± 6.6 pM, $n = 41$). Thus mixing with overlaying water-masses seems to control the concentrations of DCo along the circulation pathway of the NADW from the subarctic gyre to the south-western Atlantic, rather than scavenging processes. The lack of scavenging has previously been suggested in the central Atlantic (Noble et al., 2012), and in the Ross Sea (Saito et al., 2010). In our study we also suggest that dissolved cobalt would also behave conservatively in the deep West

BGD
10, 15951–16001, 2013

Atlantic Ocean along the thermohaline circulation. In turn the apparent scavenged profile observed in the southern part of the section (SAW) results from incursion of DCo depleted waters at the bottom of the ocean (AABW), and D-AAIW in intermediate waters.

4.2.3 Temporal variation in the Subarctic gyre

During leg 4 (2012), re-sampling of the subarctic gyre showed that the DCo concentration in the NEADW below 3000 m increased with 20.5 ± 5 pM when comparing station 5c of leg 4 with the stations 9 and 10 of leg 1, see Fig. 4a. Integrated on the thickness of the NEADW (1250 m), the DCo concentration in excess was about $25.6 \pm 6.3\,\mu mol\,m^{-2}$. Associated with these relatively high DCo concentrations, relatively high PCo concentrations were also observed below 3000 m depth (PCo > 5 pM; Figs. 4b and 5d). The transit time of the NEADW to this latitude is estimated to be around 2 yr (Fine et al., 2001). Two possible hypotheses could be invoked to explain this anomaly observed at this location: (i) intensive sediments input in the NEADW through resuspension-dissolution and/or diffusive processes during its circulation abve the seafloor; (ii) strong external input of cobalt to the Arctic surface waters transfered to the deep ocean by the formation of the NADW and its transportation through the deep large scale circulation.

Considering an input of DCo from dissolution of basalt or granit rocks of 0.054 ± 0.014 to $2 \pm 0.22\ 10^{-11}\,mol\,m^{-2}\,d^{-1}$ (Hausrath et al., 2009) and assuming this input would be continuous during the transit of the NEADW, the maximum cumulative input after two years of transit would be $7.3\,nmol\,m^{-2}$, which is three orders of magnitude lower than the excess observed. On the other hand, when considering a diffusive flux of Co from basalt of $31.1\,nmol\,m^{-2}\,d^{-1}$ estimated on the eastern Kerguelen Plateau (Bown et al., 2012a) and assuming a cumulative effect along the transportation of the water-masses, we can explain the excess in DCo observed at station 5c, since the the input would be $22.7\,\mu mol\,m^{-2}$. However the relatively poorly oxygenated waters ($O_2 < 200\,\mu M$) flowing along the Kerguelen eastern slope coupled to a relative

BGD
10, 15951–16001, 2013

high slope current (0.08 cm s^{-1}) could have enhanced sediment re-suspension (Bown et al., 2012b), and makes a comparison with our rather well ventilated bottom waters ($O_2 > 270$ µM) difficult. Anyway if sediment re-suspension and dissolution would explain the increase in DCo we would also expect to find an increase in DCo along the pathway of the NEADW, however this is not observed (Fig. 4a). Therefore we cannot use benthic input of DCo as an explanation for the enhanced DCo concentrations that we observed in 2012.

In April–May 2010 the Islandic volcano Eyjafjallajökull erupted. Considering the transit time of the NEADW of 2 yr (Fine et al., 2002) between the area of its formation in the Arctic to the latitude where the excess of DCo is observed two years after the eruption in 2012, it is thus conceivable that the DCo enrichment could be related to the dissolution of Co from these volcanic ashes. Volcanic ash emissions and subsequent deposition to the surface ocean have been reported to be a source of Co to the ocean (Frogner et al., 2001). To estimate the potential contribution of this eruption to the DCo concentrations of the surface waters in the forming area of the NEADW, we used the ash deposition flux of this eruption and the dispersion of the Icelandic ash deposits in the surface waters (Gudmundsson et al., 2012). Most of the ash deposition occured close to the vent, with 98 % of the tephra being transported less than 600–700 km from the source, and then decreasing exponentially (Gudmundsson et al., 2012). Using an ash deposition model and the mean bulk density determined by Gudmundsson et al. (2012), we estimated an ash input of $1.68 \pm 0.7 \times 10^{14}$ grams of tephra in the first 9×10^4 km^2 around Iceland, where the NEADW is formed. Using this input and a mean release of 8.76 nmol of DCo per gram of similar Iceland tephra (Frogner, 2001), we estimated a mean aeolian Co contribution to this area of around 16.3 ± 6.3 µmol m^{-2} DCo. Reported to the top-100 m, it represents an input of DCo of 163 ± 63 pM, which is at least 1.5 and up to 2.5 times the concentration observed in upper 100 m at similar latitudes in the western subarctic gyre ($DCo_{\int 100\,m} = 67.2 \pm 2$ pM), and much higher than the excess of DCo observed southward two years later (20.5 ± 5 pmol). However the theoretical DCo volcanic input and the DCo excess observed two years later at

BGD
10, 15951–16001, 2013

station 5c are in the same order of magnitude ($DCo_{volcanic\ input} = 16.3 \pm 6.3 \mu mol\ m^{-2}$; $DCo_{excess} = 25.6 \pm 6.3\ \mu mol\ m^{-2}$). It is thus conceivable that the deposition of the volcanic ashes in the surface waters in the North of the section and their dissolution along the transportation of the pathway NEADW could have caused the increase in DCo observed in 2012 in this water-mass.

4.2.4 The incursion of the Atlantic Central Waters

The highest concentrations of DCo observed at intermediate depths in the equatorial area of the section are found in the core of the Atlantic Central Waters (ACW) that originate from the Eastern Atlantic (Poole and Tomczak, 1999), and those DCo maxima correlate with the O_2 minimum (Figs. 2c, 4a, 5c). At these latitudes but in the eastern Atlantic, the O_2 depletion (Tomczak and Godfrey, 2003) and the DCo concentrations (> 150 pM; Noble et al., 2012) are even higher in the ACW compared to the western Atlantic, suggesting a zonal westward transportation of DCo across the central Atlantic ocean. Reductive dissolution in the poorly oxygenated waters, resuspension of particulate matter in the sediments along the shelfs of the eastern Atlantic, and remineralization processes are suspected to cause the DCo enrichment in the ACW observed in the eastern Atlantic (Noble et al., 2012). As suggested here above, mixing processes with the NADW can then contribute to the decrease in the DCo concentrations along the westward transportation of the ACW, whereas DCo appears to be insensitive to scavenging during transportation of this water-mass could not be discerned from water mass mixing (Noble et al., 2012). Once reaching our meridian section, the concentration of DCo continued to decrease northward in the flow of the ACW (from 93 ± 1.3 pM at 290 m, St.#15b to 73 ± 0.6 pM at 150 m, St.#36). The incursion of the ACW constitutes the major reservoir of DCo in the West Atlantic between the equatorial domain and the Caribbean basin. The decrease of DCo concentrations during the zonal and meridional transportation in the ACW could mainly be due to mixing rather than scavenging processes since no significant enrichment in PCo is observed (Figs. 4b and

BGD
10, 15951–16001, 2013

5f). Using a mean difference of DCo concentrations integrated on the W-ACW between St.#15b (9° S; 28° W) and St.#36 (8° N; 49° W) of 15 nmol m^{-3} and considering a preservation of the 4 Sv introduced by the ACW in this area (Schmitz, 1995), we estimate this decrease rate of DCo of about $(5.2 \pm 0.5) \times 10^3$ mol d^{-1} between 9° S and 8° N. Considering a surface of 2×10^6 km^2 occupied by the ACW between 9° S and 8° N this loss due to mixing processes corresponds to 2.6 ± 0.25 nmol m^{-2} d^{-1}. This loss rate compares well with the one we estimate between 10° E and 30° W using published DCo values for the eastern area (Noble et al., 2012). In the central Atlantic Ocean (10×10^6 km^2), the decrease of DCo of 56 ± 14.8 nmol m^{-3} between those longitudes which corresponds to a loss rate of 1.93 ± 0.5 nmol m^{-2} d^{-1}. However we suggest hereafter that this loss of DCo can also be partially due to vertical diffusion and advection of DCo to the surface waters especially close to the Equatorial currents where frontal systems and high turbulence were observed.

4.3 Remineralization and decoupling of the cobalt and phosphate relationship in the intermediate West Atlantic

4.3.1 Remineralization of cobalt in the Atlantic Central Waters

The highest DCo concentrations recorded along the section were observed in intermediate waters of the equatorial area (150–750 m) within the ACW (Fig. 4a), those waters that were marked by the lowest concentrations of O_2 (Fig. 2c). Hence we estimated the portion of DCo resulting from remineralization in the ACW by using the Apparent Oxygen Utilization (AOU). The AOU represents the integrated oxygen consumption by heterotrophic bacteria in the breakdown of organic matter and it is computed as the difference between the oxygen saturation concentration, which depends on thermohaline properties (Weiss, 1970), and the observed oxygen concentration. The significant correlation between AOU and DCo recorded in these waters (Fig. 8) strongly suggests that remineralization is driving the internal cycle of cobalt in these intermediate waters, as previously suggested by correlation between DCo and O_2 in other studying areas

BGD
10, 15951–16001, 2013

(Saito et al., 2004; Noble et al., 2008, 2012). This relationship is used to estimate the concentration of DCo due to the remineralization in the ACW ($[DCo]_{remineralization}$; Eq. 1), and its proportion compared to the recorded concentration of DCo ($\%DCo_{remineralized}$; Eq. 2), according to:

$$[DCo]_{remineralization} = (R_{Co:P} \times R_{P:O2} \times AOU) \quad (1)$$

$$\%DCo_{remineralized} = 100 \cdot [DCo]_{remineralization} / [DCo]_{observed} \quad (2)$$

where $R_{Co:P}$ is the stoichiometric Co : P ratio recorded in the surface waters of the equatorial area (with an average value of 27×10^{-6} M M^{-1}; Dulaquais et al., 2013), and $R_{P:O_2}$ is the stoichiometric ratio between phosphate production and oxygen consumption (e.g. $R_{P:O_2} = 1/170$ M M^{-1}; Matear and Hirst, 2003; Oschlies et al., 2008; Krishna-Murty et al., 2009).

Hence the concentration of DCo due to remineralization ($[DCo]_{remineralization}$) is estimated at about 19 ± 2.5 pM in the ACW using Eq. (1), whereas the mean DCo concentration recorded between 150 and 250 m ($[DCo]_{observed}$) is 66.6 ± 9 pM in the Equatorial area. It means that 29 % of the dissolved cobalt present in the ACW of the West Atlantic Ocean resulted from remineralization. If this remineralized DCo was only provided by transportation from the Eastern Basin, this proportion should be greater in the Eastern central Atlantic Ocean where dilution with NADW does not affect this water-mass yet. But we estimate a similar proportion in the East Atlantic ($\%DCo_{remineralized} = 28.5 \pm 4$ %) by using the DCo dataset of Noble et al. (2012). This result suggests that the DCo provided by remineralization in the West Equatorial Atlantic is likely a combination of a westward transportation of the DCo remineralized in the Eastern Atlantic basin, the cumulative remineralization along the transportation of ACW in these O_2 depleted waters and the mixing between NADW and ACW across the Equatorial Atlantic and in the Western basin.

BGD
10, 15951–16001, 2013

4.3.2 Decoupling of the relationship between cobalt and phosphate

Few studies have shown that the biological utilization of DCo can be proportional to that of phosphate (P) in the surface waters of oligotrophic provinces (Saito et al., 2004, 2010; Jakuba et al., 2008). In intermediate and deep waters, the apparent lower remineralization of DCo compared to P observed in mesopelagic waters may indicate a decoupling between the cobalt and the phosphate cycles at those depths (Bown et al., 2011). Here we further investigate such decoupling in the Equatorial area by estimating, in addition of $\%DCo_{remineralized}$ (Eq. 2), the proportion of P due to remineralization ($\%P_{remineralized}$), according to:

$$\%P_{remineralized} = 100 \cdot (R_{P:O2} \times AOU)/[P]_{observed} \quad (3)$$

In the Equatorial area, the proportion of remineralized P increases significantly with depth (by a factor 7) from the upper waters (10–150 m; $\%P_{remineralized} = 6.9 \pm 1\,\%$) to the oxygen minimum layers (150–250 m; $\%P_{remineralized} = 52 \pm 6\,\%$), whereas the proportion of remineralized DCo only increases slightly (e.g. $\%DCo_{remineralized} = 22 \pm 5\,\%$ in surface, and $29 \pm 6\,\%$ deeper) (Table 3). Deeper (> 400 m), the proportion of remineralized P and DCo are similar ($40 \pm 2\,\%$ and $37 \pm 3\,\%$, respectively). These results further support a decoupling between the remineralization of P and DCo, and suggest that it occurs in the depths of the oxygen minimum. Consequently, the increase with depth of the Co : P ratio reported in particulate material (Table 3; Sherrell and Boyle, 1992) probably results from a preferential remineralization of P compared to Co, rather than from the scavenging of Co on settling particles. The vertical distribution of PCo in this area that does not show an increase with depth (Table 3), further supports this hypothesis. Furthermore DCo is known to be strongly bound to organic ligands in the ocean (Saito and Moffett, 2001; Noble et al., 2012; Bown et al., 2012b), preventing its adsorption to settling particles.

BGD
10, 15951–16001, 2013

4.4 Physical processes impacting the distribution of dissolved cobalt in surface waters

4.4.1 Lateral advection in surface waters

The lateral advection from continental margin is thought to be a source of DCo in the open surface ocean (Bown et al., 2011, 2012b; Noble et al., 2012), but this source is still largely uncharacterized. Therefore we estimated the lateral advective DCo supply in the surface waters of the section ($FDCo_{adv}$; Eq. 4) by calculating the local geostrophic velocities (u, v; referenced 1000 dbars) based on sea level anomalies (SLA, www.aviso.oceanobs.com), and using the lateral DCo gradients (x, y) integrated in the upper 150 m (z) between two nearby stations (a, b; Eq. 5), using the following equations:

$$FDCo_{adv}(a) = GradDCo_{(x,y)} \cdot velocity_a \cdot z \quad (4)$$

$$GradDCo_{(x,y)} = [(DCo_{b\int 150\,m}) - (DCo_{a\int 150\,m})]/d_{a\rightarrow b} \quad (5)$$

where $DCo_{i\int 150\,m}$ is the mean DCo concentration integrated over the upper 150 m at station (i); $velocity_i$ is the lateral geostrophic velocity at station (i) integrated over the upper 150 m; z is equal to 150 m; and $d_{a\rightarrow b}$ is the distance between stations (a) and (b). A positive velocity is associated with a positive SLA and represents an advection from the considered station, and inversely for a negative velocity.

The dynamic structures with high lateral geostrophic velocities were generally observed in the frontal zones along the section (Table 4) and were associated with strong local currents (up to 20 cm s^{-1} as observed at 5° N), whereas relatively low velocities were estimated in the center of each oceanic domains (< 2 cm s^{-1}). However isolated events such as eddies are also identified in the center of the NASG (Table 4). The estimations of the lateral advective fluxes of DCo in surface waters show variations of more than two orders of magnitude between the different areas (Table 4). For

BGD
10, 15951–16001, 2013

instance in the center of the domains like at the station BATS, the geostrophic velocities and lateral DCo gradients were smooth resulting in negligible lateral fluxes of DCo ($-1\,\mathrm{nmol\,m^{-2}\,d^{-1}} < \mathrm{FDCo_{adv}} < 1\,\mathrm{nmol\,m^{-2}\,d^{-1}}$). On the contrary in the frontal zones where turbulence and significant lateral DCo gradients can be observed the lateral advection fluxes of DCo are relatively high in surface waters (from $-61\,\mathrm{nmol\,m^{-2}\,d^{-1}}$ to $55\,\mathrm{nmol\,m^{-2}\,d^{-1}}$, Table 4).

The DCo fluxes from lateral advection in surface waters can be important at a given station, but at the scale of a domain the impact is relatively limited, especially in the SASG. Indeed, at this scale the sum of the fluxes are low ($-3\,\mathrm{nmol\,m^{-2}\,d^{-1}} < \mathrm{FDCo} < 3\,\mathrm{nmol\,m^{-2}\,d^{-1}}$). Nevertheless the lateral advection within mesoscale structures such as eddies, can be particularly important for the transportation of DCo to interior basins, as it has been previously observed in the oligothrophic domain of the south-eastern Atlantic where inputs of DCo from continental margins were carried by Agulhas rings (Bown et al., 2011). Moreover eddies can allow exchanges of DCo between the different domains along the section, especially between the Central Atlantic and the NASG through the Equatorial current system, and between the SASG and the ECC through the MBC. Local turbulence associated with eddies can also induce local vertical advection (such as upwelling in the core of cyclonic eddies) as well as diffusion of DCo from the intermediate waters. It has been shown that such physical processes can affect the vertical distribution of DCo in surface waters (Shelley et al., 2012). All these direct and undirect effects make these dynamics structures sources or sinks of DCo to the surface layer.

4.4.2 The vertical diffusion

The vertical diffusion has been described as an important source of iron (Fe) and other nutrients to the euphotic layer, sustaining phytoplankton development in Fe-depleted areas (Law et al., 2003; Croot et al., 2003; Blain et al., 2008). In the Equatorial Atlantic this internal source of Fe may be even greater than the input of Fe from Saharan dust deposition (Rijkenberg et al., 2012). However the importance of this supply for

BGD
10, 15951–16001, 2013

DCo still has to be determined in the ocean. In the Southern Ocean and above the Kerguelen Islands the supply of DCo to surface waters by vertical diffusion has been estimated negligible, due to the small gradient in DCo concentrations between the euphotic and mesopelagic layers caused by low biological assimilation of DCo in these diatom-dominated waters (Bown et al., 2011, 2012b). By contrast strong vertical gradients in DCo concentrations between the surface and the nutricline were observed along the section in the West Atlantic Ocean, especially in the equatorial area (Fig. 5), allowing us to estimate this supply.

Briefly, the diffusion depends on the vertical gradient of DCo concentrations, the diffusion coefficient (D_T) and the turbulent diffusivity coefficient (Kz). Whereas D_T is a physico-chemical property of the component within water (molecular property), the turbulent diffusivity coefficient is solely a property of the turbulent fluid. If the vertical gradient of concentrations ($\partial DCo/\partial z$) is much higher than the lateral gradients ($\partial Co/\partial x \approx \partial DCo/\partial y$), the lateral diffusion is considered negligible (see Tables 4 and 5). Furthermore the values of Kz estimated along the section (M. Rijkenberg, NIOZ, personal communication, 2013) are three to six orders of magnitude higher than D_T, hence the molecular diffusivity is considered negligible. The highest values of Kz were found near frontal zones (M. Rijkenberg, NIOZ, personal communication, 2013) where strong geostrophic velocities are observed. One to two orders of magnitude lower turbulent diffusivities were found in the subtropical domains, coherent with lower turbulence of the water column and lower wind stress.

The intrusion of the ACW in the southern side of the equatorial area and its northward flow along the coast of South America through the Guyana and Caribbean Currents (Poole and Tomczak, 1999) transports relatively high DCo within the mesopelagic layer and at the bottom of the euphotic layer (100–250 m) between 10° S and 10° N (Fig. 4a). Because the assimilation of DCo in surface waters is also relatively high at those latitudes (Dulaquais et al., 2013), strong DCo vertical gradients are generated between the surface and intermediate waters (Figs. 4a, 5). For instance the DCo vertical gradient can be as high as 0.31 nmol m^{-3} m^{-1} in the equatorial area at 9° S. By contrast the

BGD
10, 15951–16001, 2013

vertical gradients are generally smooth in the subtropical domains and in the subarctic gyre ($<0.07\,\mathrm{nmol\,m^{-3}\,m^{-1}}$). Combining the vertical gradients with the K_z pattern it is obvious that the vertical diffusion DCo supply is expected to be higher in the frontal zones of the equatorial area than in the other domains. To further assess the role of the vertical diffusion on the distribution of DCo in surface waters, we estimated the DCo vertical diffusion flux ($\mathrm{FDCo_{diffusion}}$) in the different domains using the following equation:

$$\mathrm{FDCo_{diffusion}} = -(K_z + D_\mathrm{T}) \cdot (\partial \mathrm{DCo}/\partial z) \quad (6)$$

with

$$10^3 < (K_z/D_\mathrm{T}) < 10^6 \quad (7)$$

The DCo supply to the euphotic layer by vertical diffusion (Table 5) varies by two orders of magnitude between the frontal zones (e.g. $7\,\mathrm{nmol\,m^{-2}\,d^{-1}}$ in the north subtropical frontal zone) and the center of the subtropical domains (e.g. $<0.07\,\mathrm{nmol\,m^{-2}\,d^{-1}}$ in the oligotrophic domains). In the frontal systems, the highest turbulence (Table 5) combined with a significant vertical gradient of DCo concentrations causes high vertical diffusion fluxes of DCo into the surface waters. In the equatorial area the high diffusive input of DCo is mainly due to high vertical gradients of DCo induced by the incursion of the Eastern South ACW enriched in DCo. This input may well sustain the growth of the cyanobacteria present in the equatorial domain towards 15° N (Tovar-Sanchez et al., 2006). By contrast this input keeps relatively low in the oligotrophic domains mainly due to lower turbulent fluids. Therefore the vertical diffusion does not appear to be the dominant flux to sustain the cyanobacteria population in the oligotrophic domains. External sources like dust and rivers (Tovar-Sanchez, et al., 2006; Dulaquais et al., 2013), and/or eddies that locally increase the turbulence (Noble et al., 2008) may rather be invoked to respond to the absolute requirement to cobalt of this dominant population in those domains (Saito and Moffett, 2001).

BGD
10, 15951–16001, 2013

5 Conclusions

Large-scale observation of the deep distribution of dissolved cobalt as first assessed in this work allows to further understand the role of physical and remineralization processes in the deep cycle of cobalt. In deep-waters DCo behaves conservatively along water-masses transportation through the West Atlantic. Mixing and dilution of deep water-masses, rather than scavenging of DCo onto settling particles, generate the meridional decrease of DCo along the southward large-scale circulation in the deep West Atlantic. This finding contrasts with previous interpretations that DCo would have to be scavenged along the thermohaline circulation to explain the deep inter-basins fractionation (Bruland and Lohan, 2003). In addition the conservative behaviour of DCo allows the persistence of relatively high concentrations in the core of the LSW and low concentrations in the underlaying AABW, hence generating the apparent scavenged profile of DCo observed in the deep waters of the West Atlantic. It also allows large-scale transportation of external cobalt sources to interior basins, such as the 2010 Icelandic volcanic eruption which is depicted by relatively high DCo concentrations in the core of the NEADW at 51° S. In addition the DCo enriched intermediate waters can act as internal inputs of DCo into the surface waters through dynamic processes. Eddies and dynamics structures such as equatorial surface jets could play a major role in the fertilization of surface water in DCo through vertical diffusion and lateral advection. The input of DCo by the vertical diffusion is particularly enhanced in the equatorial domain where the incursion of the Atlantic Central Waters at intermediate depths that transports high DCo concentrations compared to the surface, generates a strong vertical DCo gradient. However these processes are still poorly constrained and further work is required to better constrain these fluxes.

Next to physical processes, reductive processes notably those linked to the oxygenation of the water-masses also play a major role in the deep cycle of DCo. The ACW characterized by relatively low O_2 indeed exhibits the highest DCo concentrations encountered along the section, hence constituting the major reservoir of DCo in the West

BGD
10, 15951–16001, 2013

Atlantic. The relatively low oxygenation of these waters may have promoted the stabilization of DCo in the westward flow of the ACW across the Atlantic Ocean, whereas physical processes do not prevent DCo to decrease along the route of these waters due to mixing and dilution with other water-masses containing less DCo and to vertical diffusion to surface waters. In addition the significant correlation between DCo concentrations and the apparent oxygen utilization found in these waters further indicate that remineralization (abiotic and biotic) is driving the internal cycle of cobalt in these intermediate waters. The remineralization of DCo was not proportional to that of phosphate in these intermediate waters, unlike the biological uptake of both DCo and P previously reported in oligotrophic surface waters (e.g. Saito et al, 2002; Noble et al., 2008; Bown et al., 2011). This decoupling leads to an enrichment of Co relative to P in the settling particles, mainly due to the preferential remineralization of P rather than a preferential scavenging of Co. Observations at regional and basin scales both indicate that scavenging of DCo onto particles may not be driven the distribution of dissolved cobalt in the deep ocean. Records of truly particulate cobalt will further help in revealing the role of particles in the deep cycle of cobalt.

Acknowledgements. We are indebted to the Captains, Officers and Crew Members of the R/V *Pelagia* and R.S.S. *James Cook*: without their exceptional support, this large ocean section would not have been possible. We are most grateful to H. J. W. de Baar, the Coordinator of the Dutch Project, and to L. Gerringa and M. Rijkenberg, the Chief Scientists of the cruises. We warmly thank J. van Ooijen, K. Bakker, E. van Weerlee, S. Ossebaar for the analyses of nutrients, as well as S. Ober, M. Laan, S. van Heuven, S. Asjes and L. Wuis for providing high quality CTD data. This investigation was supported by the GEOTRACES-GEOSECS revisited in the West Atlantic project coordinated by M. Boye and funded by the French LEFE-CYBER National Program of the Institut National des Sciences de l'Univers (INSU). We also acknowledge the European COST-Action ES801 for funding a Short Term Scientific Mission to G. Dulaquais to join the last cruise. The Université de Bretagne Occidentale (UBO) and the Région Bretagne are supporting the PhD fellowship of G. Dulaquais. This investigation is a contribution to the international GEOTRACES program.

BGD
10, 15951–16001, 2013

References

Aparicio-Gonzalez, A., Duarte, C. M., and Tovar-Sanchez, A.: Trace metals in deep ocean waters: A review, J. Marine Systems, 100, 26–33, 2012.

Behl, W. K. and Toni, J. E.: Anodic oxidation of cobalt in potassium hydroxide electrolytes, Journal of Electroanalytical Chemistry and Interfacial Electrochemistry, 31, 63–75, 1971.

Biller, D. V. and Bruland, K. W.: Analysis of Mn, Fe, Co, Ni, Cu, Zn, Cd, and Pb in seawater using the Nobias-chelate PA1 resin and magnetic sector inductively coupled plasma mass spectrometry (ICP-MS), Mar. Chem., 130, 12–20, 2012.

Blain, S., Quéguiner, B., Armand, L., Belviso, S., Bombled, B., Bopp, L., Bowie, A., Brunet, C., Brussaard, C., Carlotti, F., Christaki, U., Corbière, A., Durand, I., Ebersbach, F., Fuda, J.-L., Garcia, N., Gerringa, L., Griffiths, B., Guigue, C., Guillerm, C., Jacquet, S., Jeandel, C., Laan, P., Lefèvre, D., Lo Monaco, C., Malits, A., Mosseri, J., Obernosterer, I., Park, Y.- H., Picheral, M., Pondaven, P., Remenyi, T., Sandroni, V., Sarthou, G., Savoye, N., Scouarnec, L., Souhaut, M., Thuiller, D., Timmermans, K., Trull, T., Uitz, J., van Beek, P., Veldhuis, M.,Vincent, D., Viollier, E., Vong, L., and Wagener, T.: Effect of natural iron fertilization on carbon sequestration in the Southern Ocean, Nature, 446, 1070–1074, 2007.

Bowie, A. R. and Lohan M. C.: Analysis of iron in seawater, in Practical Guidelines for the Analysis of Seawater, edited by: Wurl, O., Taylor and Francis, Boca Raton, Fla., chap. 12, 235–257, 2009.

Bown, J., Boye, M., Baker, A., Duvieilbourg, E., Lacan, F., Le Moigne, F., Planchon, F., Speich, S., and Nelson, D. M.: The biogeochemical cycle of dissolved cobalt in the Atlantic and the Southern Ocean south off the coast of South Africa, Mar. Chem., 126, 193–206, doi:10.1016/j.marchem.2011.03.008, 2011.

Bown, J., Boye, M., and Nelson, D. M.: New insights on the role of organic speciation in the biogeochemical cycle of dissolved cobalt in the southeastern Atlantic and the Southern Ocean, Biogeosciences, 9, 2719–2736, doi:10.5194/bg-9-2719-2012, 2012a.

Bown, J., Boye, M., Laan, P., Bowie, A. R., Park, Y.-H., Jeandel, C., and Nelson, D. M.: Imprint of a dissolved cobalt basaltic source on the Kerguelen Plateau, Biogeosciences, 9, 5279–5290, doi:10.5194/bg-9-5279-2012, 2012b.

Boyd, P. W. and Ellwood, M. J.: The biogeochemical cycle of iron in the ocean, Nature Geosciences, 3, 675–682, 2010.

BGD
10, 15951–16001, 2013

Bruland, K. W. and Lohan, M. C.: The control of trace metals in seawater. In the Oceans and Marine Geochemistry, Treatise on Geochemistry, edited by: Elderfield, H., Elsevier, 6, 2003.
Cannizzaro, V., Bowie, A. R., Sax, A., Achterberg, E. P., and Worsfold, P. J.: Determination of cobalt and iron in estuarine and coastal waters using flow injection with chemiluminescence detection, The Analyst, 125, 51–57, 2000.
De Baar, H. J. W., Timmermans, K. R., Laan, P., De Porto, H. H., Ober, S., Blom, J. J., Bakker, M. C., Schilling, J., Sarthou, G., Smit, M. G., and Klunder, M.: Titan: A new facility for ultraclean sampling of trace elements and isotopes in the deep oceans in the international GEOTRACES program, Mar. Chem., 111, 4–21, doi:10.1016/j.marchem.2007.07.009, 2008.
Ellwood, M. J.: Wintertime trace metal (Zn, Cu, Ni, Cd, Pb and Co) and nutrient distributions in the subantarctic zone between 40–52° S; 155–160° E. Mar. Chem., 112, 107–117, 2008.
Fine, R. A., Rhein, M., and Andrie, C.: Using a CFC effective age to estimate propagation and storage of climate anomalies in the deep western North Atlantic Ocean, Geophys. Res. Lett., 29, 2227–2230, 2002.
Fitzwater, S. E., Johnson, K. S., Gordon, R. M., Coale, K. H., and Smith, W. O.: Trace metal concentrations in the Ross Sea and their relationship with nutrients and phytoplankton growth, Deep-Sea Res. Part II, Topical Studies in Oceanography, 47, 3159–3179, 2000.
Frogner, P., Gislason, S. R., and Oskarsson, N.: Fertilizing potential of volcanic ash in ocean surface water, Geology, 29, 487–490, 2001.
Gislason, S. R., Hassenkam, T., Nedel, S., Bovet, N., Eiriksdottir, E. S., Alfredsson, H. A., Hem, C. P., Baloggh, Z. I., Dideriksen, K., Oskarsson, N., Sigfusson, B., Larsen, G., and Stipp, S. L. S.: Characterization of Eyjafjallajokull volcanic ash particles and a protocol for rapid risk assessment, Proc. Nat. Acad. Sci., 108, 7307–7312, 2011.
Gladyshev, S., Arhan, M., Sokov, A., and Speich, S.: A hydrographic section from South Africa to the southern limit of the Antarctic Circumpolar Current at the Greenwich meridian, Deep-Sea Res. Pt. I, 55, 1284–1303, 2008.
Grasshoff, K., Kremling, K., and Ehrhardt, M.: Methods of seawater analysis, Verlag Chemie GmbH, Weinheim, 419 pp., 1983.
Gudmundson, M. T., Thodarson, T., Höskuldsson, A., Larsen, G., Björnsson, H., Prata, F. J., Oddson, B., Magnusson, E., Högnadottir, T., Petersen, G. N., Hayward, C. L., Stevenson, J. A., and Jonsdottir, I.: Ash generation and distribution from the April-May 2010 eruption of Eyjafjallajokull, Iceland, Nature Scientifc Reports, 2, 572, doi:10.1038/srep00572, 2012.

BGD
10, 15951–16001, 2013

Jakuba, R. W., Moffett, J. W., and Dyhrman, S. T.: Evidence for the linked biogeochemical cycling of zinc, cobalt, and phosphorus in the western North Atlantic Ocean, Global Biogeochem. Cy., 22, GB4012, doi:10.1029/2007GB003119, 2008.
Knauer, G. A., Martin, J. H., and Gordon, R. M.: Cobalt in Northeast Pacific Waters, Nature, 297, 49–51, 1982.
Hausrath, E. M., Neaman, A., and Brantley, S. L.: Elemental release rates from dissolving basalt and granite with and without organic ligands, Am. J. Sci., 309, 633–660, doi:10.2475/08.2009.01, 2009.
Heggie, D. and Lewis, T.: Cobalt in pore waters of marine sediments, Nature, 311, 453–455, 1984.
Krishnamurthy, A., Moore, J., Mahowald, N., Luo, C., Doney, S., Lindsay, K., and Zender, C.: Impacts of increasing anthropogenic soluble iron and nitrogen deposition on ocean chemistry, Global Biogeochem. Cy., 23, GB3016, doi:10.1029/2008GB003440, 2009.
Law, C. S., Abraham, E. R., Watson, A. J., and Liddicoat, M.: Vertical diffusion and nutrient supply to the surface mixed layer of the Antarctic Circumpolar Current, J. Geophys. Res., 108, 3272, doi:10.1029/2002JC001604, 2003.
Martin, J. H., Gordon, R. M., and Fitzwater, S. E.: Iron in Antarctic waters, Nature, 345, 156–158, 1990.
Martin, J. H., Fitzwater, S. E., Gordon, R. M., Hunter, C. N., and Tanner, S. J.: Iron, primary production and carbon nitrogen flux studies during the JGOFS North-Atlantic Bloom Experiment, Deep-Sea Res. Pt. I – Topical Studies in Oceanography, 40, 115–134, 1993.
Matear, R. and Hirst, A.: Long-term changes in dissolved oxygen concentrations in the ocean caused by protracted global warming, Global Biogeochem. Cycles, 17, 12427–12432, doi:10.1029/2002GB001997, 2003.
Mather, R., Reynolds, S., Wolff, G., Williams, R. G., Torres-Valdes, S., Woodward, E. M. S., Landolfi, A., Pan, X., Sanders, R. W., and Achterberg, E.: Phosphorus cycling in the North and South Atlantic Ocean subtropical gyres, Nat. Geosci., 1, 439–443, 2008.
Milne, A., Landing, W., Bizimis, M., and Morton, P.: Determination of Mn, Fe, Co, Ni, Cu, Zn, Cd and Pb in seawater using high resolution magnetic sector inductively coupled mass spectrometry (HR-ICP-MS), Anal. Chim. Acta, 665, 200–207, 2010.
Moffett, J. W. and Ho, J.: Oxidation of cobalt and manganese in seawater via a common microbially catalyzed pathway, Geochimica and Cosmochimica Acta, 60, 3415–3424, 1996.

BGD
10, 15951–16001, 2013

Murphy, J. and Riley, J. P.: A modified single solution method for the determination of phosphate in natural waters, Anal. Chim. Acta, 27, 31–36, 1962.
Noble, A. E., Saito, M. A., Maiti, K., and Benitez-Nelson, C. R.: Cobalt, manganese, and iron near the Hawaiian Islands: A potential concentrating mechanism for cobalt within a cyclonic eddy and implications for the hybrid-type trace metals, Deep-Sea Res. Pt. II, 55, 1473–1490, doi:10.1016/j.dsr2.2008.02.010, 2008.
Noble, A. E., Lamborg, C. H., Ohnemus, D. C., Lam, P. J., Goepfert, T. J., Measures, C. I., Frame, C. H., Casciotti, K. L., DiTullio, G. R., Jennings, J., and Saito, M. A.: Basin scale inputs of cobalt, iron, and manganese from the Benguela-Angola front to the South Atlantic Ocean, Limnol. Oceanogr., 57, 989–1010, 2012.
Oschlies, A., Schulz, K., Riebesell, U., and Schmittner, A.: Simulated 21st century's increase in oceanic suboxia by CO_2-enhanced biotic carbon export, Global Biogeochem. Cy., 22, GB4008, doi:10.1029/2007GB003147, 2008.
Peterson, R. G. and Stramma, L.: Upper-level circulation in the South Atlantic Ocean. Prog. Oceanogr., 26, 1–73, doi:10.1016/0079-6611(91)90006-8, 1991.
Pohl, C., Croot, P. L., Hennings, U., Daberkow, T., Budeus, G., and von der Loeff, M. R.: Synoptic transects on the distribution of trace elements (Hg, Pb, Cd, Cu, Ni, Zn, Co, Mn, Fe, and Al) in surface waters of the Northern- and Southern East Atlantic, J. Marine Sys., 84, 28–41, 2011.
Poole, R. and Tomczak, M.: Optimum multiparameter analysis of the water mass structure in the Atlantic Ocean thermocline, Deep Sea Res., 46, 1895–1921, 1999.
Reid, J. L.: On the total geostrophic circulation of the South-Atlantic Ocean – flow patterns, tracers, and transports, Prog. Oceanogr., 23, 149–244, 1989.
Reid, J. L.: On the total geostrophic circulation of the North Atlantic Ocean: Flow patterns, tracers and transports, Prog. Oceanogr., 33, 1–92, 1994.
Rijkenberg, M. J. A., Steigenberger, S., Powell, C. F., van Haren, H., Patey, M. D., Baker, A. R., and Achterberg, E. P.: Fluxes and distribution of dissolved iron in the eastern (sub-) tropical North Atlantic Ocean, Global Biogeochem. Cy., 26, GB3004, doi:10.1029/2011GB004155, 2012.
Saito, M. A. and Moffett, J. W.: Complexation of cobalt by natural organic ligands in the Sargasso Sea as determined by a new highsensitivity electrochemical cobalt speciation method suitable for open ocean work, Mar. Chem., 75, 49–68, 2001.

BGD
10, 15951–16001, 2013

Saito, M. A. and Goepfert, T. J.: Zinc–cobalt colimitation of *Phaeocystis antarctica*, Limnol. Oceanogr., 53, 266–275, 2008.
Saito, M. A. and Moffett, J. W.: Temporal and spatial variability of cobalt in the Atlantic Ocean, Geochim. Cosmochim. Acta, 66, 1943–1953, 2002.
Saito, M. A., Moffett, J. W., and DiTullio, G. R.: Cobalt and nickel in the Peru upwelling region: A major flux of labile cobalt utilized as a micronutrient, Global Biogeochem. Cy., 18, GB4030, doi:10.1029/2003GB002216, 2004.
Saito M. A., Rocap, G., and Moffett, J. W.: Production of cobalt binding ligands in a Synechococcus feature at the Costa Rica Upwelling Dome, Limnol. Oceanogr., 50, 279–290, doi:10.4319/lo.2005.50.1.0279, 2005.
Saito, M. A., Goepfert, T. J., Noble, A. E., Bertrand, E. M., Sedwick, P. N., and DiTullio, G. R.: A seasonal study of dissolved cobalt in the Ross Sea, Antarctica: micronutrient behavior, absence of scavenging, and relationships with Zn, Cd, and P, Biogeosciences, 7, 4059–4082, doi:10.5194/bg-7-4059-2010, 2010.
Shelley, R. U., Zachhuber, B., Sedwick, P. N., Worsfold, P. J., and Lohan, M. C.: Determination of total dissolved cobalt in UV-irradiated seawater using flow injection with chemiluminescence detection, Limnol. Oceanogr., 8, 352–362, doi:10.1029/2009JC005880, 2010.
Shelley, R. U., Sedwick, P. N., Bibby, T. S., Cabedo-Sanz, P., Church, T. M., Johnson, R. J., Macey, A. I., Marsay, C. M., Sholkovitz, E. R., Ussher, S. J., Worsfold, P. J., and Lohan, M. C.: Controls on dissolved cobalt in surface waters of the Sargasso Sea: Comparisons with iron and aluminum. Global Biogeochem. Cy., 26, GB2020, doi:10.1029/2011GB004155 2012.
Sherrell R. M. and Boyle E. A.: The trace metal composition of suspended particles in the oceanic water column near Bermuda, Earth Planet. Sci. Lett., 111, 155–174, 1992.
Schmitz Jr., W. J.: On the interbasin-scale thermocline circulation, Rev. Geophys., 33, 151–173, 1995.
Strickland, J. D. H. and Parsons, T. R.: A pracitcal handbook of seawater analysis. First Edition, Fisheries Research Board of Canada, Bulletin, No. 167, p. 65, 1968.
Tomczak, M. and Godfrey, J. S.: Regional Oceanography: an Introduction, 2nd edition, Pergamon, Oxford, 422 pp., 2003.
Tovar-Sanchez, A. and Sañudo-Wilhelmy, S. A.: Influence of the Amazon River on dissolved and intra-cellular metal concentrations in Trichodesmium colonies along the western bound-

BGD
10, 15951–16001, 2013

ary of the sub-tropical North Atlantic Ocean, Biogeosciences, 8, 217–225, doi:10.5194/bg-8-217-2011, 2011.
Tovar-Sanchez, A., Sanudo-Wilhelmy, S. A., Kustka, A. B., Agusti, S., Dachs, J., Hutchins, D. A., Capone, D. G., and Duarte, C. M.: Effects of dust deposition and river discharges on trace metal composition of *Trichodesmium spp.* in the tropical and subtropical North Atlantic Ocean, Limnol. Oceanogr., 51, 1755–1761, 2006.
Vega, M. and van den Berg, C. M. G.: Determination of cobalt in seawater by catalytic adsorptive cathodic stripping voltammetry, Anal. Chem., 69, 874–881, 1997.
Webb, D. J. and Suginohara, N.: Oceanography: Vertical mixing in the ocean, Nature, 409, 37, 2001.
Weiss, R.: The solubility of nitrogen, oxygen, and argon in water and seawater, Deep Sea Res., 17, 721–756, 1970.
Whitworth III, T. and Nowlin Jr., W. D.: Water masses and currents of the Southern Ocean at the Greenwich Meridian, J. Geophys. Res., 92, 6462–6476, 1987.
Wong, G. T. F., Pai, S. C., and Chung, S. W.: Cobalt in the western Philippine Sea, Oceanol. Acta, 18, 631–638, 1995.
You, Y.: Quantitative estimate of Antarctic Intermediate Water contributions from the Drake Passage and the southwest Indian Ocean to the South Atlantic, J. Geophys. Res., 107, 107C2, doi:10.1029/2001JC000880, 2002.

BGD
10, 15951–16001, 2013

Table 1. Comparison of dissolved cobalt analyses obtained in the UV-oxidized samples by the FIA-Chemiluminescence method used in the present study with consensus values reported by the Sampling and Analysis of iron (SAFe) and GEOTRACES programs. Water samples provided by SAFe and GEOTRACES from surface waters (SAFe S and GEOTRACES S) and deep waters (SAFe D1 and D2, and GEOTRACES D) were analyzed. Errors are given as standard deviation from average values.

Sample	DCo measured (pM)	Consensus value (pM)
SAFe S	5.1 ± 2.2 (n = 25)	4.8 ± 1.20
SAFe D1	42.3 ± 1.4 (n = 15)	45.4 ± 4.7
SAFe D2	44.2 ± 1.7 (n = 25)	45.7 ± 2.9
GEOTRACES S	29.8 ± 2 (n = 35)	31.8 ± 1.1
GEOTRACES D	63.2 ± 2.3 (n = 25)	65.2 ± 1.2

BGD
10, 15951–16001, 2013

Table 2. Averaged dissolved cobalt concentration (DCo) and standard error (SE) obtained in the different water-masses encountered along the West Atlantic GEOTRACES-A02 section: the North East Atlantic Deep Water (NEADW), Labrador Sea Water (LSW), North Atlantic Deep Water (NADW), Western Atlantic central waters (W-ACW), North West Antarctic Bottom Water (NW-AABW), South West Antarctic Bottom Water (SW-AABW) and Drake Antarctic Intermediate Water (D-AAIW).

Water-mass	DCo (pM)	SE (pM)	*n*
NEADW	54.3	2.7	24
LSW	68.8	3.2	38
NADW	61.8	8	204
W-ACW	>85	4.4	7
NW-AABW	44.52	4.8	42
SW-AABW	39.29	4.4	45
D-AAIW	53.7	4	11

BGD
10, 15951–16001, 2013

Table 3. Mean dissolved cobalt concentration (DCo; pM), mean apparent particulate cobalt concentration (PCo; pM), and pourcentages of dissolved cobalt and phosphate produced by remineralization (respectively DCo_{rem} and P_{rem} %) (see text for the calculation). The particulate ratios of Co : P ($(Co/P)_{in\ particles}$; $\mu M\ M^{-1}$) recorded in the West Atlantic (Sherrell and Boyle, 1992) are also indicated for comparison. Errors are given as standard deviation from average values.

Depth (m)	DCo (pM)	PCo (pM)	DCo_{Rem} (%)	P_{Rem} (%)	$Co/P_{in\ particles}$ $\mu M\ M^{-1}$
10–150	31.6 ± 12 ($n = 37$)	4 ± 3 ($n = 13$)	22 ± 5	6.9 ± 1	403 ± 128
150–250	66 ± 9 ($n = 18$)	2.6 ± 2.7 ($n = 7$)	29 ± 6	52 ± 6	2718 ± 1180
400–800	72 ± 6 ($n = 19$)	1.6 ± 1.3($n = 8$)	37 ± 3	40 ± 2	5420 ± 2440

BGD
10, 15951–16001, 2013

Table 4. Lateral gradient of dissolved cobalt (Grad $DCo_{\int 150\,m}$; 10^{-5} nmol m^{-3} m^{-1}), and lateral advective fluxes of dissolved cobalt ($FDCo_{adv}$; nmol m^{-2} d^{-1}) generated by local geostrophic lateral advection (Fw_{Geo}; cm s^{-1}) are given in the upper 150 m for several sampling stations corresponding to key-dynamical structures or domains.

Location	Structure	Grad $DCo_{\int 150\,m}$	Fw_{Geo}	$FDCo_{adv}$
St. 5 (37° W; 60° N)	Center of SAG	+0.39	−0.23	−0.11
St. 15 (50° W; 37.5° N)	Anti-cyclonic eddy	+1.37	−9.73	−17.28
St. 21 (BATS)	Center of NASG	−0.39	−0.16	+0.08
St. 25 (67° W; 25° N)	cyclonic eddy	−0.15	+13.28	−2.54
St. 36 (48.9° W; 7.8° N)	NEC	−3.21	+10.03	−41.67
Btw St. 37–38 (45° W; 5° N)	ECC	−2.1	−19.99	+54.82
Btw St. 16b–17b (28.5° W; 5° S)	SEC	−0.6	+3.92	−3.19
St. 12b (32.7° W; 22.5°§)	Center SASG	+0.62	+1.15	+0.92
St. 6b (42.5° W; 40° S)	MBC	−1.58	−7.76	+15.85
Btw St. 2b–3b (48° W; 48° S)	Malvinas current	+0.02	−7.54	−0.23

BGD
10, 15951–16001, 2013

Table 5. Vertical dissolved cobalt gradient (ΔDCo/Δz100–300 m; nmol m^{-3} m^{-1}), mean $Kz_{100-300\,m}$ (cm^2 s^{-1}) and vertical dissolved cobalt fluxes from the mesopelagic layer to the euphotic layer (FDCo$_{\text{vertical diff.}}$; nmol m^{-2} d^{-1}) at few stations representative of the different areas crossed along the section (see text for the details of the calculations).

Location	ΔDCo/Δz100–300 m	Kz	FDCo$_{\text{vertical diff.}}$
St. 15 (50° W; 37.5° N)	0.115	7	+6.96
St. 21 (BATS)	0.069	0.08	+0.05
St. 26 (65.5° W; 23.3° N)	0.12	0.07	+0.07
St. 36 (48.9° W; 7.8° N)	0.291	2.44	+6.13
St. 15b (28° W; 9° S)	0.305	1.2	+3.16
St. 12b (32.7° W; 22.5° S)	0.062	0.11	+0.06
St. 6b (42.5° W; 40° S)	0.084	3.7	+2.69

BGD
10, 15951–16001, 2013

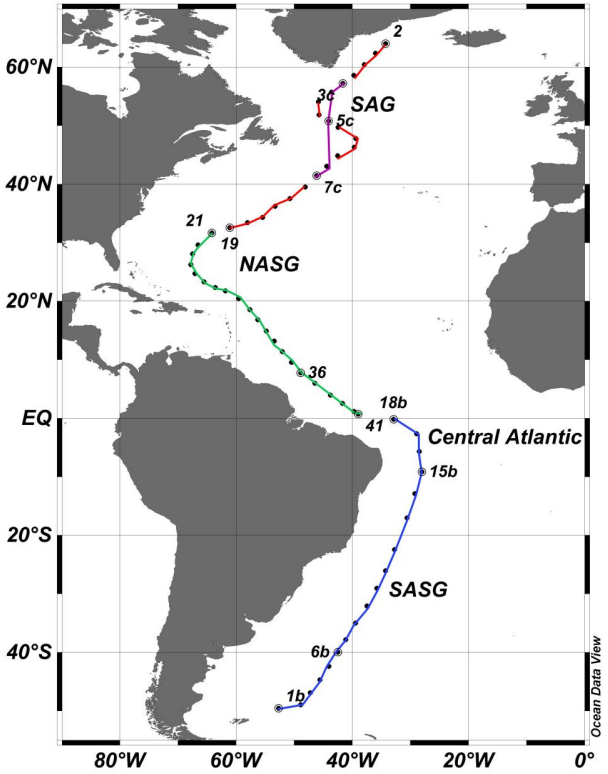

Fig. 1. GEOTRACES-A02 cruises track along the West Atlantic Ocean. Sampling locations of the four Legs are shown (Leg 1 in red line from St. 2 to St. 19, Leg 2 in green line from St. 21 to St. 41, Leg 3 in blue line from St. 1b to 18b and Leg 4 in purple line from St. 3c to 7c).

BGD
10, 15951–16001, 2013

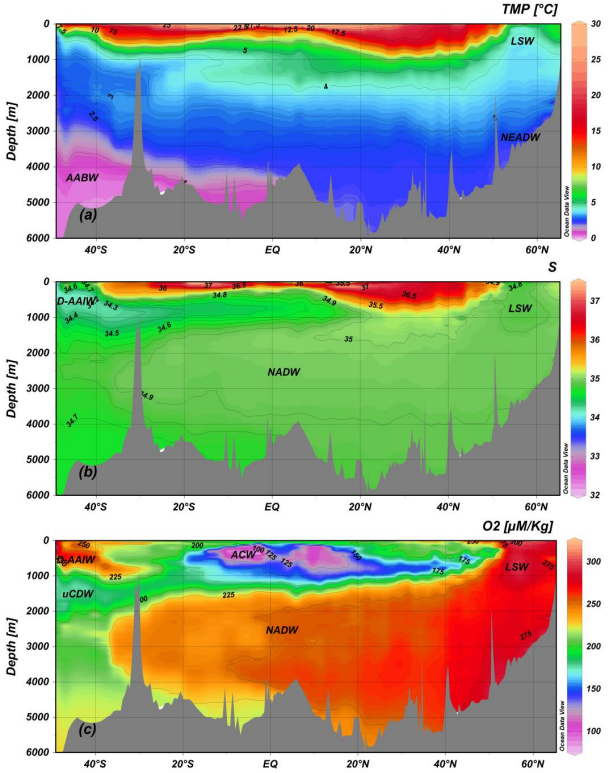

Fig. 2. Interpolated vertical sections of **(a)** temperature (TMP), **(b)** salinity (*S*) and **(c)** dissolved oxygen (O_2) along the section in the West Atlantic, based on CTD data. The different water-masses: LSW, NEADW, NADW, ACW, AABW, D-AAIW and uCDW are identified by their physical features and are indicated in the figure.

BGD
10, 15951–16001, 2013

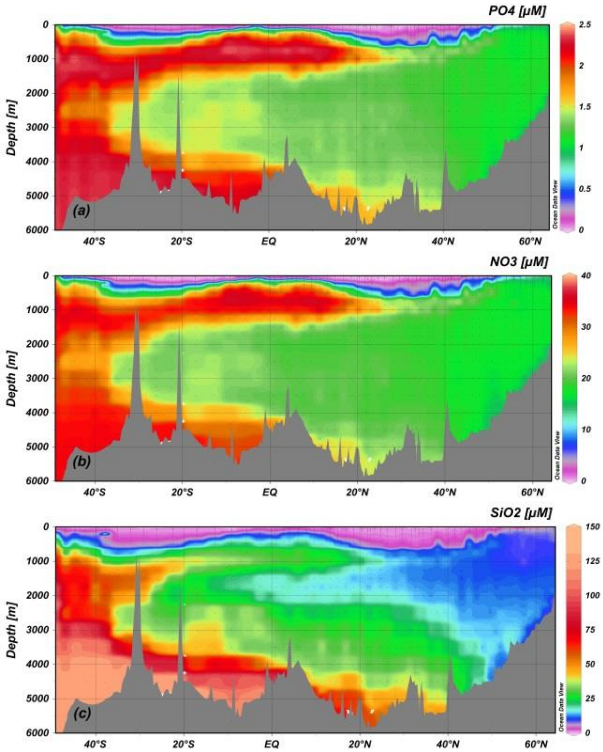

Fig. 3. Interpolated vertical sections of **(a)** phosphate, **(b)** nitrate and **(c)** silicates based on 1440 analysis of water-column samples collected and measured by NIOZ along the NL-GA02 section.

BGD
10, 15951–16001, 2013

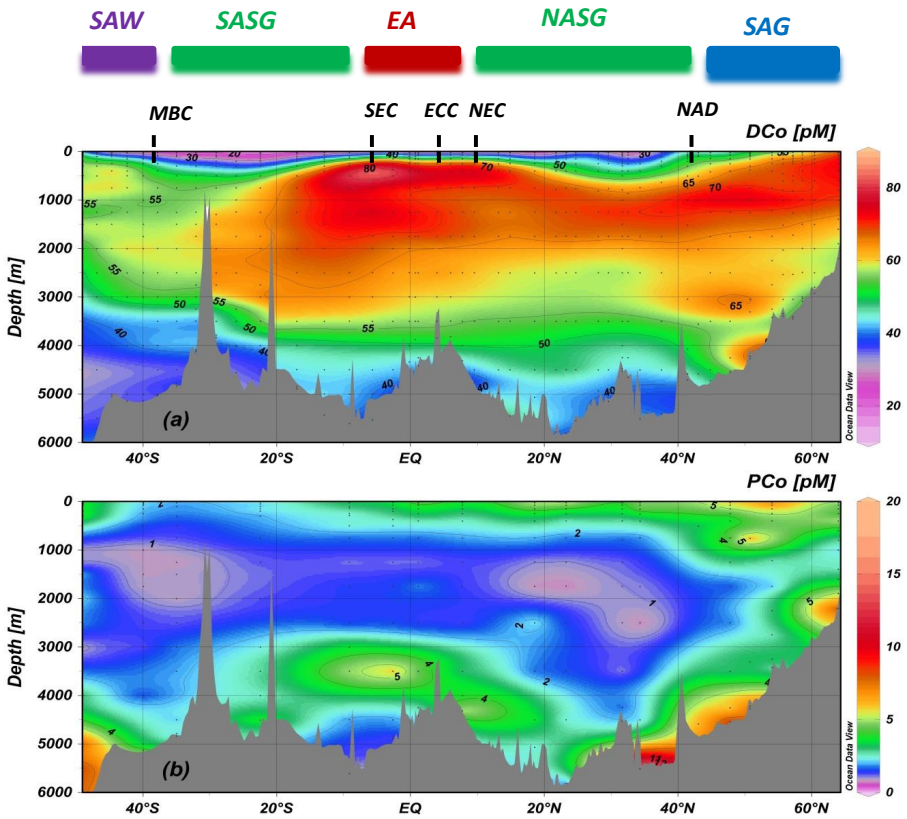

Fig. 4. Interpolated vertical sections of **(a)** dissolved cobalt (DCo, pM) and **(b)** apparent particulate cobalt (PCo, pM) based on 675 analyses for DCo and 203 analyses for PCo, along the GEOTRACES-A02 section in the West Atlantic. The domains of SAG, NASG, EA, SASG and SB are characterized by the macro-nutrients concentrations and by the surface currents (e.g. NAD, NEC, SEC, and MBA).

BGD
10, 15951–16001, 2013

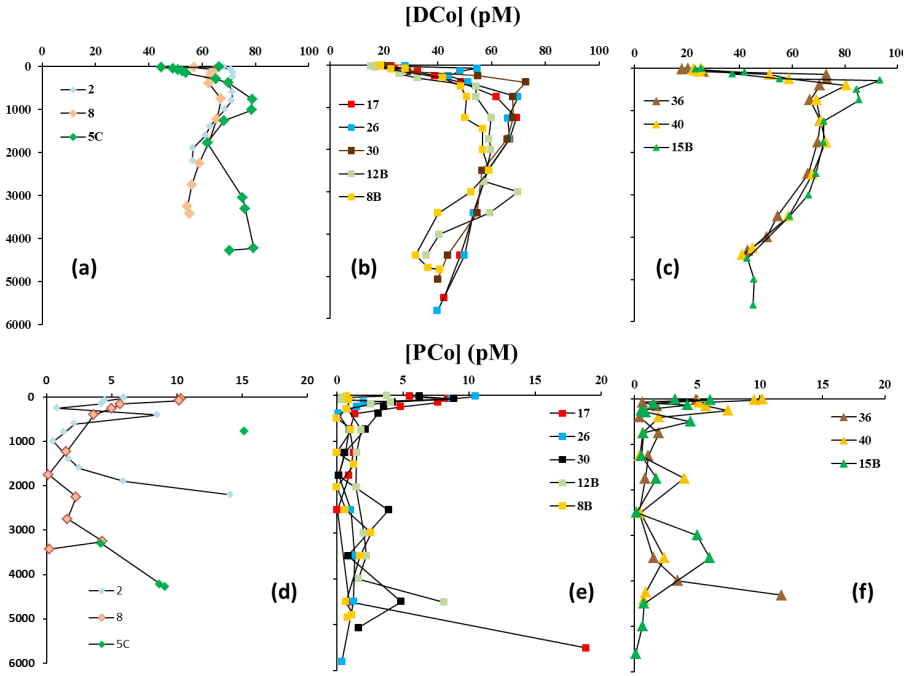

Fig. 5. Typical vertical distribution of dissolved (DCo) and apparent particulate (PCo) cobalt against depth in the different biogeochemical domains: in the SAG, DCo **(a)** and PCo **(d)** are shown for St. 2 (64 degree N; 34.25° W), St. 8 (54° N; 45.84° W) and St. 5c (50° N; 44° W); in the north and south subtropical domains DCo **(b)** and PCo **(e)** are shown at St. 17 (34.3° N; 55.4° W), St. 26 (23° N; 65.55° W), St. 30 (18.5° N; 57.6° W), St. 12b (22.47° S; 32.7° W) and St. 8b (35° S; 39.4° W); and in the equatorial area DCo **(c)** and PCo **(f)** are presented at St. 36 (7.8° N; 48.9° W), St. 40 (1° N; 39.7° W) and St. 15b (9° S; 28° W).

BGD
10, 15951–16001, 2013

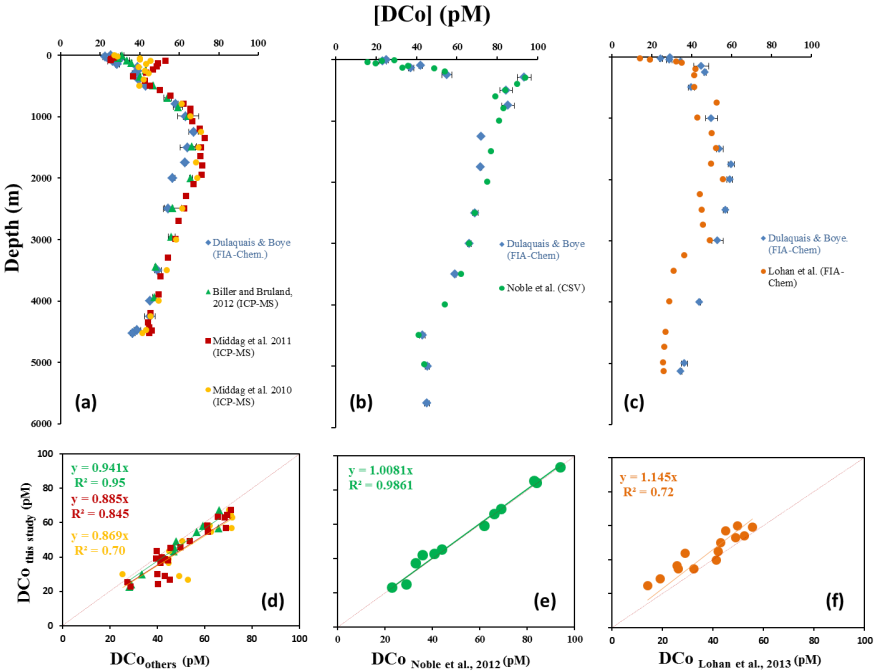

Fig. 6. Intercomparison of DCo datasets at the cross-over station BATS **(a, d)** between this study (blue diamonds) and ICP-MS method by Biller and Bruland [2008] (green triangles) and by Middag,Bruland et al. (2013) (yellow dots = samples from the 2010 Dutch GEOTRACES-A02 cruise; red squares = samples from the 2011 American GEOTRACES-A03 cruise); at the cross-over station located at 9° S **(b, e)** between this study (blue diamonds) and the CSV method by Noble et al. (2012) (green dots); and at the cross-over station at 40° S **(c, f)** between this study (blue diamonds) with FIA-Chem. method by Lohan et al. (2013) (orange dots = samples from the 2010 English GEOTRACES-A10 cruise).

BGD
10, 15951–16001, 2013

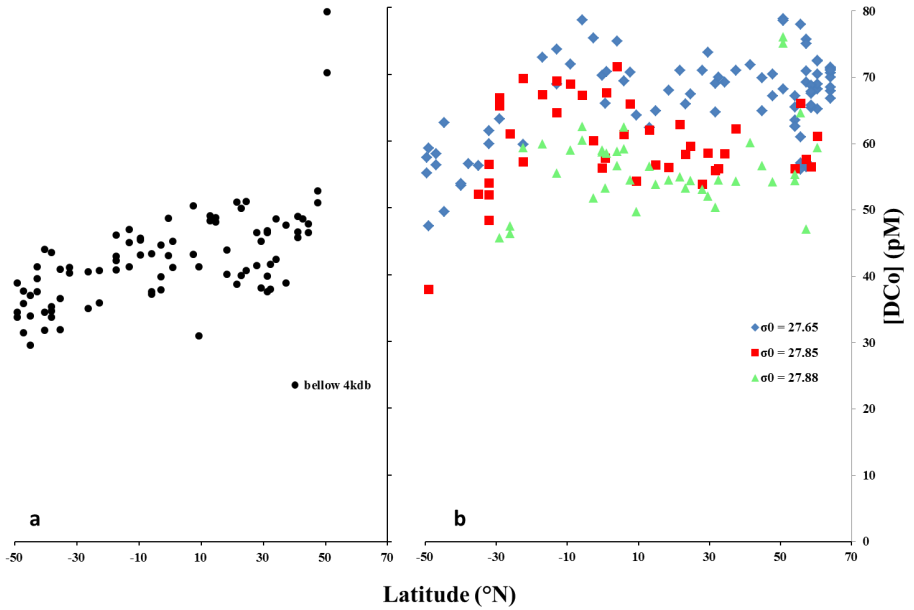

Fig. 7. Scatter plots of dissolved cobalt concentrations (DCo) along the GEOTRACES-A02 section below 4 kdb (**a**; dark squares) and at three potential density anomaly: $\sigma 0$ = $27.65 \pm 0.1\,kg\,m^{-3}$ (**b**; blue diamonds), $\sigma 0$ = $27.85 \pm 0.02\,kg\,m^{-3}$ (**b**; red squares) and $\sigma 0$ = $27.88 \pm 0.015\,kg\,m^{-3}$ (**b**; green triangles).

BGD
10, 15951–16001, 2013

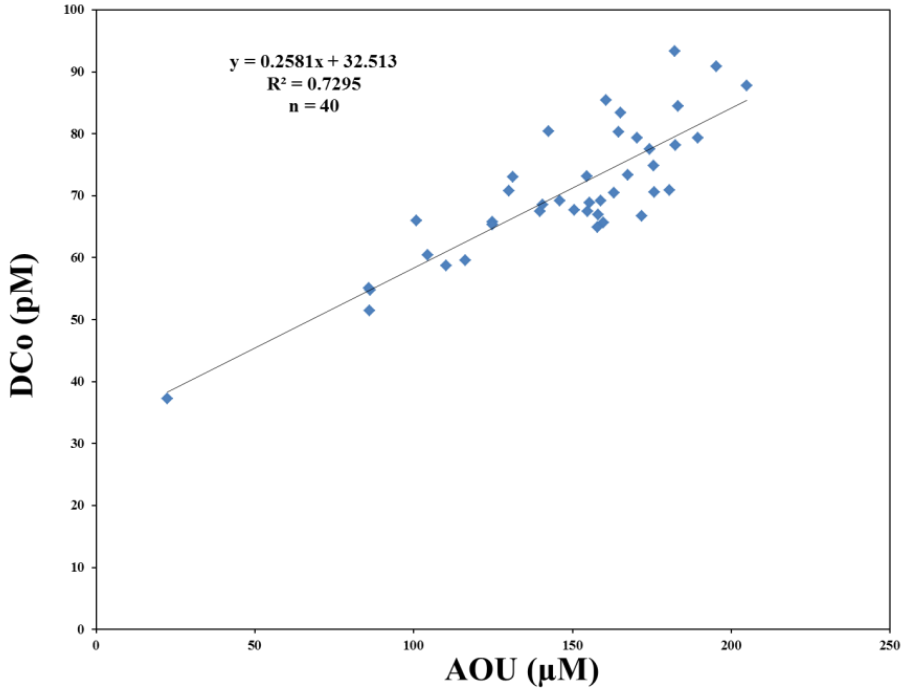

Fig. 8. Relationship among the concentrations of dissolved cobalt (DCo) and the apparent oxygen utilization (AOU) in the intermediate waters of the equatorial area (150–750 m).

BGD
10, 15951–16001, 2013